Title	Development of treatment and diagnostic techniques for dental caries using light based on minimal intervention
Author(s)	近藤, 聡太
Citation	大阪大学, 2024, 博士論文
Version Type	VoR
URL	https://doi.org/10.18910/96080
rights	
Note	

Doctoral Dissertation

Development of treatment and diagnostic

techniques for dental caries using light

based on minimal intervention

Sota Kondo

December 2023

Graduate School of Engineering,

Osaka University

Supervisor： Associate Professor Hisanao Hazama
(Medical Beam Physics Laboratory)

Vice supervisors： Professor Fuminobu Sato
(Quantum Beam and Biomaterials Engineering Laboratory)
Professor Hiroaki Muta
(Energy and Environmental Materials Laboratory)

Abstract

Caries is a disease caused by decalcification due to organic acids such as lactic acid produced by metabolism and degradation of sugar in a dental plaque on a tooth surface. Especially, root caries is a dental disease that affects more than one in three persons in the geriatric population. In recent years, a minimally invasive dental treatment for teeth corresponding to a concept of minimal intervention was strongly desired. As a minimally invasive treatment, a caries selective removal had not been achieved with the conventional microsecond-pulsed Er:YAG laser due to the thermal effect. In this study, the possibility of the caries selective removal with nanosecond-pulsed Q-switched Er:YAG laser satisfying the thermal confinement condition was suggested. However, the caries selective removal could be possible with the dentin hardness as a caries status, and the methods to measure dentin hardness have not existed for clinical use or been still qualitative. Therefore, this study developed a dentin hardness measurement method to objectively and quantitatively evaluate the activity and progress of root caries in a clinical setting. This technique was called "HAMILTOM." With the demonstration of HAMILTOM using bovine dentins with different demineralization times, the correlation between the dentin hardness measured by HAMILTOM and measured by the Vickers hardness tester was evaluated. Moreover, the mechanism of dentin hardness measurements and the invasiveness to dentin were evaluated in this study in order to interpret the dentin hardness measured by HAMILTOM physically.

Chapter 1 provided the background of caries and root caries. The trend of minimal intervention for caries treatment was provided. To realize the philosophy of minimal intervention, the significance of a treatment of selective removal for caries and a method to objectively and quantitatively measure the dentin hardness to prevent unnecessary treatment were presented.

Chapter 2 provided the possibility of selective removal for caries with nanosecond-pulsed Q-switched Er:YAG laser at the wavelength of 2.94 μm to develop a less-invasive laser caries treatment using the laser. The characteristics of laser ablation to dentin slices were examined and compared between the Q-switched Er:YAG laser with a pulse duration of 80–130 ns and the free-running Er:YAG laser with a pulse duration of 200–300 μs without water spray. The results confirmed that the ablation selectivity of the caries model was observed at a low peak power density and the suppression of dental pulp necrosis due to the temperature increase by the laser irradiation could be possible. However, in the clinical situation, the condition and the degree or progression of caries are various, which suggested that the optimal condition of laser irradiation for each caries could be unclear. The caries selective removal could be difficult to achieve in the clinical situation without the information of dentin hardness.

Chapter 3 provided the proof of principle of the optical dentin hardness measuring device using bovine dentin. In order to evaluate the activity and progress of caries in a clinical setting, an

objective and quantitative method to evaluate dentin hardness which can be used easily in the clinical setting had to be established. In this study, the new device was proposed to easily measure the hardness of *in vivo* teeth using a light-emitting diode. HAMILTOM quantified the hardness of dentin from the contact projection area (dark area) between the indenter and dentin when the indenter was pressed into the dentin. The results of the demonstration of HAMILTOM confirmed that the correlation between the dark area and the Vickers hardness.

Chapter 4 discussed the mechanism of dentin hardness measurements and the invasiveness to dentin by HAMILTOM because the measurement mechanism for quantitative dentin hardness evaluation had remained unclear. The mechanism was discussed by the result of the difference between dark areas and indentation areas, and the invasives to dentin was discussed by comparing the invasiveness to dentin with the conventional dental probe. The results suggested that the dentin hardness (dark area) measured by HAMILTOM included not only the deformation of dentin but also the exuded water from dentin. The comparison of the indentation depths suggested that palpation by a dental probe caused the larger indentation depth than HAMILTOM.

Chapter 5 provides the overall conclusion. HAMILTOM has the potential of a new diagnostic device for caries and a strong support for the realization of selective removal for caries to measure the dentin hardness in a clinical setting.

Table of contents

Chapter 5: Conclusion   77

List of Figures

injection using waterproof abrasive papers and a lapping film.

3.2 Schematic illustration of the HAMILTOM handpiece device. Image of the tip of the glass indenter was projected onto the CMOS camera with a threefold magnification using the LED light. By applying a load to the tip of the indenter, the lens barrel rotated around the rotation axis. Then the lens barrel and the housing applied the load to the load sensor. When the load reached the set value, the CMOS camera acquired an image of the indenter.

3.3 Principle of measuring the dark area projected between the glass indenter and dentin. When the indenter contacted with dentin, a total internal reflection of LED light did not occur, and the indenter at the contact area appeared dark because the refractive indices of the glass indenter and dentin were similar. (a) Dark area for sound dentin was small at a constant load of 50 gf (~0.49 N) because the sound dentin was hard. (b) The dark area for demineralized dentin is larger for the set load because the demineralized dentin was softer than sound dentin.

3.4 Image of the experimental system for the measurement of dark areas with HAMILTOM. HAMILTOM was fixed at the base first, and the dentin sample was located directly below the indenter of HAMILTOM. The stage was slowly raised vertically, and an image acquired with the CMOS camera when the load reaches 50 gf (~0.49 N). At the same time, the load was measured by an electronic balance to confirm the accuracy of the load measured by the load sensor.

3.5 Typical images of reflected light from the glass indenter taken with the CMOS camera. Images for dentin samples with different demineralization times (0, 0.25, 0.5, 0.75, 1, 2, 4, 6, 12, or 24 h) were shown for group 1. The scale bar showed the length of 500 µm.

3.6 Dark area, Vickers hardness, and their relationship for the samples in group 1. Each graph showed the mean and standard deviation of three measurements. (a) Changes in the dark area with different demineralization times. (b) Changes in the Vickers hardness with different demineralization times. (c) Relationship between the dark area and the Vickers hardness. Dashed line showed the approximate expression. A determination coefficient was also shown for (c).

3.7 Typical images of reflected light from the glass indenter taken with the CMOS camera. Images for dentin samples with different demineralization times (0, 0.25, 0.5, 0.75, 1, 2, 4, 6, 12, or 24 h) were shown for group 2. The scale bar showed the length of 500 µm.

3.8 Dark area, Vickers hardness, and their relationship for the samples in group 2. Each graph

showed the mean and standard deviation of three measurements. (a) Changes in the dark area with different demineralization times. (b) Changes in the Vickers hardness with different demineralization times. (c) Relationship between the dark area and the Vickers hardness. Dashed line showed the approximate expression. A determination coefficient was also shown for (c).

3.9 Relationship between the Vickers hardness $H_{V.tester}$ of the samples in group 2 measured with the Vickers hardness tester and the Vickers hardness $H_{V,HAMILTOM}$ calculated by the dark area of the samples in group 2 with the calibration curve obtained from the result of measurement with the samples in group 1. The mean and standard deviation of three measurements, approximate expression (dashed line), and determination coefficient were shown.

4.1 Schematic illustration of the HAMILTOM handpiece used in this study. Image of the resin indenter tip was projected onto the CMOS camera with a threefold magnification using LED light. First, the reference image was obtained by pressing the reference acquisition button. By applying a load to the indenter tip, the lens barrel rotates around the rotation axis, and the lens barrel and the housing apply a load to the capacitive load sensor. Then CMOS acquires an image of the indenter when the load reaches a predetermined value.

4.2 Image of the experimental system to measure dark areas by HAMILTOM used in this study. HAMILTOM was fixed at the base with the two points, and the dentin sample was placed directly below the indenter. When the dark area was measured, the stage was slowly raised vertically, and an image was acquired with the CMOS camera when the load reaches 50 gf (~ 0.49 N). To verify the accuracy of the load measured by the sensor, the load was also measured by an electronic balance.

4.3 Image of the experiment to create indentations with a dental probe by a dentist. To moisten the dentin sample, it was immersed in saline for at least 24 hours before the experiment. Then the excess surface moisture was blown off with air prior to indentation creation. The dentist applied the same force as a clinical setting to create indentations on the dentin surface using a dental probe and created the indentations at three random positions for each sample.

4.4 SEM images and mapping of Ca content of the cross-section surface of each dentin sample with the different demineralization time (0.25, 0.5, 0.75, 1, 2, 4, 6, 12, or 24 h) measured with the energy dispersive X-ray spectrometer attached to the SEM used in this study. The top side of the images illustrates the dentin sample surface on which the indentations were created in this study.

theoretical formulas. The dark areas were calculated from the theoretical formula shown in **3.2.4** (6) and the Vickers hardness were calculated from the theoretical formula shown in **3.2.5** (7).

4.13 The relationship between the dark area measured by HAMILTOM and Vickers hardness measured in this study. Dotted line showed the approximate expression. A determination coefficient was shown.

List of Tables

Chapter 1

Introduction

1.1 Caries

The world's population is not only increasing but it is also aging. According to the World Health Organization (WHO), 1 in 6 people will be 60 years or older by 2030, and the world's population over 60 years of age will reach 2.1 billion by 2050 [1]. As life expectancy of the aging population increases, people retain their teeth for longer [2], causing the risk increase of developing caries. Caries is caused by decalcification due to organic acids such as lactic acid produced by metabolism and degradation of sugar in a dental plaque on a tooth surface where there are causative bacteria related to the demineralization. Dental caries lesions are classified into five zones from the extent or structure of demineralization, which are zone of decomposed dentin, zone of decalcification with bacterial invasion, zone of decalcification without bacterial invasion, zone of dentinal sclerosis and zone of fatty degeneration from the most severe surface of tooth. Moreover, they are classified into two layers that are 'outer layer of caries dentin' with bacterial infection, which is not remineralizeable and perceivable, and 'inner layer of caries dentin' without bacterial infection which is able to remineralize [3]. Its boundary is between the zone of decalcification with bacterial invasion and that without bacterial invasion.

Basically, caries does not heal naturally and caries are progressive. In early caries localized to enamel, remineralization occurs due to redeposition of minerals in saliva or demineralized minerals. Although the condition could be maintained for a long time, the condition deteriorates to dental pulpitis with severe pain if the lesion progressed and reached the deep part of dentin, and if it was unattended. Ultimately, it ends up with tooth extraction. Therefore, it is desirable to take proper treatment before the disease progresses to pulpitis and restore oral function and sensuousness [3].

During the last five decades, measures to combat dental caries have been developed, tested and implemented in many populations worldwide, and are thought to have provided benefits to millions of people [4]. In spite of the huge effort made, a large part of the population in the world still suffers from the disease of caries [5], which are the main causes of tooth loss. In Japan, the number of people who have caries has been decreasing year by year since 1980 and the trend has continued in recent years [6]. However, the prevalence of dental caries is still very high. With regard to permanent teeth, it was reported that the percentage of those who currently have caries was lower than 10 % in the age group between 5 and 10 years old but more than 80 % in the age group between 25 and 85

years old increasing with age. Especially, it was close to 100 % among people whose age are between 35 and 55 years old [7]. It is clear from many epidemiological investigations that chewing ability for all foods can be maintained by 20 or more teeth remaining, and a remarkable decrease in the chewing ability is observed when the residual teeth become less than 20 [8]. In addition, a value of 51.2 % has been reported as a percentage of people who have more than 20 teeth at the age of 80 [7], and the loss of teeth due to age is still a public health problem. In conventional caries treatments, the main point was put on the complete removal of caries, but the trend has been changing into conservation of tooth or pulp with minimal invasion caused by cutting from the viewpoint of conservation restoration science [9]. Because of the trend change, a minimally invasive dental treatment for teeth corresponding to a concept of minimal intervention (MI) advocated by Federation Dentaire Internationale (FDI) is strongly desired in recent years.

1.2   Root caries

Root caries is a dental disease which affects more than one in three persons in the geriatric population [10]. Root caries are more often found on the exposed root surfaces or the margin of the cementoenamel junction [11]. Root caries is defined as a cavitation below the cementoenamel junction not including the adjacent enamel, usually discolored, softened ill-defined and involving both cementum and underlying dentin [12]. Enamel contains about 90 % minerals; therefore, the enamel is stronger and more acid-resistant than any other dental tissue [13]. In comparison, cementum and dentin are composed of about 45 % to 50 % and 70 % inorganic materials, respectively [14,15]. The cementum and dentin have higher solubility compared with enamel due to their higher content of magnesium and carbonate [16]. Compared to enamel, cementum and dentin on a root surface are more susceptible to caries progression and is more likely to cause tooth loss. Root caries begins with demineralization of cementum after exposure of the root surface due to gingival recession, and spreads to the dentin. Cementum is a tissue similar to dentin and has lower acid resistance than enamel, making it more susceptible to caries. Caries progresses against the dentin by collapsing and shedding the cementum, exposing a wide area of dentin. The thickness of the cementum in cervical area is thin, approximately 20–50 μm, and most root caries identified by inspection is dentin caries. Therefore, this study focused on dentin because it is considered important to evaluate the progression of root caries to dentin.

The treatment of root caries is much more difficult than that of the crown because the cutting of root surface caries could break the tooth, and the proximity to the gingiva could make cement filling difficult. Therefore, it is important to assess the progression of root caries through diagnosis to prevent severe root caries.

1.3　Minimal intervention

MI is the basic philosophy of dental treatments in general advocated by FDI in 2002, and has following five concepts in principle [17, 18].

① Modification of the oral flora

   It is important to prevent infection by removing plaque and restricting intake of sugar since caries is an infectious disease.

② Patient education

   It is necessary to explain the formation of dental caries and how to prevent being caries through guidance on diet and cleaning in a mouth to patients.

③ Remineralization of non-cavitated lesions of enamel and dentin

   The course of the caries should be observed with remineralization therapy because such caries has been proved to stop or treat its progress.

④ Minimal operative intervention of cavitated lesions

   In cutting of dental substances, natural tooth should try to be preserved as much as possible and, only enamel that seems to be broken and infected dentin should be cut.

⑤ Repair of defective restorations

   Removal of restorations could result in some removal of healthy tooth and the size of the cavity could increase. Instead of repairing the entire restoration, it is also an option to repair it.

In the cutting treatment of caries dentin, 'minimally invasive caries treatment' is important as mentioned in ④ in order to make the diseased tooth function longer. 'Minimally invasive caries treatment' not only minimizes cutting amount for healthy teeth but also implies reliable removal of caries dentin, and therefore setting criteria for cutting or non-cutting is important.

At the moment, an infected tooth removal with a caries dentin detection solution is the most reliable clinical method. The caries dentin detection solution dyes the layer infected by bacteria which is called outer layer of caries dentin red, and cutting is conducted with the dyeing as a guide [19]. However, the remineralized caries dentin or sound dentin is removed by cutting until the dyeing disappears. For this reason, it is not necessary to get rid of all the stained parts, and it is regarded as the end point to be cut as far as the part which is dyed light pink [20]. Also, it is inevitable that a judgment on the staining status is based on a subjective view [21], and the method of discriminating the infected tooth to be removed remains problematic.

In addition, there are problems remaining in terms of devices for cutting a tooth which is a dental hard tissue. According to the principles of MI, ideally a medical device should minimally invade sound dentin and be able to remove infected dentin selectively without excess or deficiency.

However, such an ideal device in clinical use does not exist at the moment, and traditional manual cutting tools and rotating turbines are used in treatments.

1.4   Selective removal for caries with a laser

From the perspective of minimal intervention for caries treatment, a medical device which minimally invades sound dentin and be able to remove infected dentin selectively without excess or deficiency is ideal and desired. The absorption spectra of human sound and carious dentin in the mid-infrared wavelength were shown in the previous study [22]. Although the absorption spectra of caries dentin did not show absorption band associated with PO stretching because hydroxyapatite was eluted during the demineralization process, the absorption bands with OH stretching and amide bands were stronger in caries dentin than in sound dentin. Since carious dentin contains more water than sound dentin, caries selective removal could be possible with a laser considered by taking advantage of the difference in absorption spectra due to OH stretching vibrations exhibited by the wavelength of 2.94 µm. Especially, the caries selectivity of removal with minimal intervention could be achieved with the irradiation with Er:YAG laser at the wavelength of 2.94 µm without water spray, by using the amount of light absorption caused by differences in water content between sound dentin and caries dentin.

1.5   Quantitative diagnosis with a light

The selective removal for caries could be an ideal treatment in accordance with the basic philosophy of dental treatments of minimal intervention, and the possibility of the selective removal for caries with a laser needs to be investigated in this study. However, the most minimal-intervention approach, I believe, is to preserve natural tooth or teeth that do not require treatment as much as possible without treatment.

Root caries is diagnosed by inspection and palpation basically. The indicators contain the color, surface texture, and hardness of the lesion [23,24]. Although the diagnosis is based on inspection and palpation, there is no clear color change in the initial root caries [25], and palpation is performed using a dental probe. Hence, the diagnosis is qualitative depending on dentists. Hardness of dentin becomes softer with the progress of caries, but the diagnosis using a dental probe depends on the dentist's sensitivity to pressure changes when inserting and removing the probe. In fact, the kappa statistics for the inspection and palpation for root caries are as low as 30 % to 51 % [26], which is very low. Therefore, a method to objectively and quantitatively measure the dentin hardness and evaluate the activity and progress of root caries in a clinical setting is strongly required to realize the most minimal-intervention approach preventing unnecessary caries treatment.

1.6   Aim of this study

This study aimed to develop a treatment with the caries selectivity of removal using a laser. Since carious dentin contains more water than sound dentin, caries selective removal could be possible with a laser considered by taking advantage of the difference in absorption spectra due to OH stretching vibrations exhibited by the wavelength of 2.94 µm. The characteristics of laser ablation to dentin slices were examined and compared between the Q-switched Er:YAG laser with a pulse duration of 80–130 ns and the free-running Er:YAG laser with a pulse duration of 200–300 µs without water spray. Furthermore, as the most minimal-intervention approach, a diagnostic method to objectively and quantitatively measure the dentin hardness with a light was aimed to prevent unnecessary caries treatment. The demonstration of the basic principle of an optical dentin hardness measurement device using bovine dentin samples with different demineralization times, and the mechanism of dentin hardness measurements using HAMILTOM and the invasiveness to dentin were evaluated.

1.7   Outline of this dissertation

To develop a technique for selective removal of caries with a laser, the characteristics of laser ablation to dentin slices were examined and compared between the nanosecond-pulsed Q-switched Er:YAG laser with a pulse duration of 80–130 ns and the microsecond-pulsed free-running Er:YAG laser with a pulse duration of 200–300 µs without water spray in Chapter 2. To develop a diagnostic method to objectively and quantitatively measure the dentin hardness with a light, the demonstration of the basic principle of an optical dentin hardness measurement device using bovine dentin samples with different demineralization times were presented in Chapter 3. In Chapter 4, the mechanism of dentin hardness measurements using HAMILTOM and the invasiveness to dentin were discussed. The overall conclusion was provided in Chapter 5.

Chapter 2

In vitro study on nanosecond-pulsed *Q*-switched Er:YAG laser-induced selective removal for caries dentin

2.1 Introduction

2.1.1 History of lasers in dentistry

Seodol Maiman successfully oscillated a ruby laser using ruby as an active substance for the first time in the world in 1960 [27]. In 1964, Goldman and Stern already tried to form cavities of extracted teeth using lasers [28,29]. However, the lasers developed in the early days caused a serious thermal damage to the dentin, and it was supposed that a dental treatment with a laser would be impossible. However, due to the technical improvement of laser equipment, CO_2 laser was applied to dental treatment early in the 1960's, which showed acquisition of acid resistance to enamel [30], superior hemostatic effect on soft tissue, few damages on surrounding tissues, and pain reduction [31–33]. But, since the wavelength band of 9–11 μm has strong absorption into hydroxyapatite, cracks and carbonization due to the high thermal effect, and melting of the tooth surface have been reported, which suggested that the laser treatment was unsuitable for hard tissue cutting. In addition, Nd:YAG laser with a wavelength of 1.06 μm has a small absorption of tooth substance, penetrates the hard tissues and reaches the pulp which is damaged by the thermal effect. Consequently, Nd:YAG laser was not suitable for cutting hard tissues as well as CO2 laser [34]. Therefore, currently both CO2 laser and Nd:YAG laser are mainly applied to soft tissues [35].

For cutting hard tissues, Er:YAG laser is the only laser which has been applied for caries treatment in Japan, and is used in clinical situation. Er:YAG laser is a solid-state laser developed by Zharikov et al. in 1974, and has a wavelength of 2.94 μm. In 1989, Hibst, Keller and Chino et al. reported that it was possible to evaporate hard tissues by Er:YAG laser [36, 37], demonstrating the possibility of caries removal by laser. The wavelength of Er:YAG laser is 2.94 μm which is very

strongly absorbed by water, and it is able to cut teeth by evaporating water on the tooth surface. In clinical use, it is possible to cut teeth safely without causing cracks or thermal damage of the pulp by using water spray for cooling. The caries treatment using Er:YAG laser is reported to have less unpleasant symptoms for patients [38], because uncomfortable noise or vibration during the treatments are extremely less than a conventional rotating cutting tool [39, 40]. Hibst and Keller et al. reported that more than 80 % of patients wanted to receive the laser treatment instead of the rotating cutting tool after the laser treatment [41]. In addition, since noise or vibration which give discomfort to patients are extremely small, it is expected as an effective method for children and people with disabilities. Laser dental treatment has been prevailing and has covered by insurance. 20 points of caries tooth painless cavity formation addition is newly established for painless caries removal by laser irradiation in 2008 revision of medical fee, and it was raised to 40 points in 2010.

Moreover, Er:YAG laser can be applied not only to the hard tissues but also soft tissues such as gingiva, tooth root, bone tissue and titanium dental implants [42]. Applications for various clinical situations such as a soft tissue treatment, a periodontal treatment, a periodontal surgery treatment, and a treatment for peri-implant inflammation have been tried worldwide [43–47]. However, clinical application to bone tissue such as alveolar bone removal and the reshaping has been approved by the Food and Drug Administration (FDA), but they have not been approved in Japan yet.

2.1.2 Caries treatment with Er:YAG laser

In MI treatment for caries, selective removal of infected tooth tissue is desired. Since carious dentin contains more water than sound dentin, the possibility of caries selective cutting was considered by taking advantage of the difference in absorption spectra due to OH stretching vibrations exhibited by the wavelength of 2.94 µm. In the past, the ablation with Er:YAG laser was selective for caries because the caries contained much water [48], and the opening of the dentinal tubule as seen on the surface of dentin ablated by Er:YAG laser was thought to be suitable for repair system with composite resin [49–51]. Therefore, MI therapy with Er:YAG laser was advertised. However, since the reaction between Er:YAG laser and water spray is dominant in the treatment, the fact is that the selective ablation of caries has not been achieved. With Er:YAG laser irradiation with water spray, the caries selectivity of ablation was not observed, and it has been reported that the variation in the ablation volumes were the largest among various cutting methods and the risks that infected tooth remained or excessive cutting happened were very high [52, 53]. In addition, it is reported that laminate structure or formation of a fragile thermal denatured layer was observed on the surface of dentin after the Er:YAG laser irradiation, which could cause the decrease in adhesive strength of composite resin [54]. Although the composite resin does not fall off shortly after it is repaired on the laser-irradiated dentin, in the long term the deterioration of the restoration could be accelerated causing hyperesthesia and secondary caries [55]. Furthermore, the efficiency of cutting

with Er:YAG laser is much lower than high-speed rotating cutting tools, and the extension of treatment time is a serious problem [56]. On the other hand, the irradiation with Er:YAG laser without water spray, the caries selectivity of ablation could be achieved by using the amount of light absorption caused by differences in water content between sound dentin and caries dentin. However, the water spray is indispensable in the actual caries treatment with Er:YAG laser to suppress the thermal effect caused by the laser irradiation. However, the sound dentin is also ablated due to the dominancy of light absorption to sprayed water resulting in loss of caries selectivity of ablation. Therefore, a new laser dental treatment with less thermal effect which is able to achieve the selective ablation of caries needs to be developed.

2.1.3 Possibility of selective removal for caries with *Q*-switched Er:YAG laser

In the caries treatment with Er:YAG laser, water spray is used because it induces a cavitation effect in water on dentin [57] and cooling due to the thermal effect of the laser in the treatment process. Without water spray or with water spray at 1 mL/min, thermal damage such as carbonization and increased temperature occurs on an irradiated dentin surface [58]. However, sound dentin is also ablated under the treatment with water spray, and the selectivity of the caries is sometimes poor for dental caries removal [59]. In a recent study with a diode-pumped Er:YAG laser operating with a short pulse duration of 20–100 μs, selective removal only between healthy enamel and demineralized dentin was shown [60]. It is necessary to achieve a treatment with a lower thermal effect and less water spray.

The thermal confinement condition is an important index when assessing the thermal effect. The thermal confinement condition is satisfied when the pulse duration is much shorter than the thermal relaxation time. The range of the temperature increase in a tissue is limited to the light-absorption region defined by the light-penetration depth when the thermal confinement condition is satisfied. The thermal relaxation time is the period where the temperature increase at the optical penetration depth becomes 1/e of the surface temperature increase. The thermal relaxation time at the wavelength of free-running Er:YAG laser (2.94 μm) without water spray is 142 μs for sound dentin and 58.3 μs for caries dentin [61]. On the one hand, the pulse duration of the free-running Er:YAG laser is approximately 200–300 μs, which shows that the thermal confinement condition is not satisfied and the heat spreads to the surrounding tissues of dentins. In recent studies, a pulse variable Er:YAG laser with a pulse duration between 20 and 100 μs has been utilized to irradiate dentin [59, 62–64], but the pulse durations are still too long to satisfy the thermal confinement condition.

On the other hand, a *Q*-switched Er:YAG laser has a pulse duration around 100 ns, and the laser is able to satisfy the thermal confinement condition with the expected suppression of the thermal effect. A previous study confirmed that the irradiation marks from the heat-denatured layer on dentin are greatly reduced using a *Q*-switched Er:YAG laser [65]. Water spray is used during treatment with

the free-running Er:YAG laser to prevent the thermal denaturation of the laser-irradiated dentin surface and the occurrence of cracks due to the thermal influence. However, the Q-switched Er:YAG laser has a possibility to be a laser treatment with no water spray allowing effective use of the difference in the optical absorption coefficients between sound and caries dentin. Therefore, a laser treatment with the Q-switched Er:YAG laser is expected to be a caries-selective treatment.

2.1.4 Purpose of the study in this chapter

The purpose of the study in this chapter is to develop a less-invasive laser caries treatment using the Q-switched Er:YAG laser for achieving a caries treatment with minimal intervention. Here, the characteristics of laser ablation to dentin slices were examined and compared between the Q-switched Er:YAG laser with a pulse duration of 80–130 ns and the free-running Er:YAG laser with a pulse duration of 200–300 µs without water spray.

2.2 Materials and Methods

2.2.1 Sample preparation

Bovine sound dentin slices were used as samples in this study. The size of the samples was $10 \times 10 \times 1$ mm^3. The processes for preparation included cutting sound anterior dentins using a cutter (MC-201 M; Maruto, Tokyo, Japan) and polishing with a no. 600 waterproof abrasive paper (26-4738; Maruto). The surface of samples was perpendicular to the direction of the dentinal tubules. Caries models were created by immersing sound dentin slice samples into 0.1-Mlactic acid solution (M5R3990; Nacalai Tesque, Kyoto, Japan) at 37 °C, which stirred for 24 h [66]. The caries models were preserved in distilled water after the artificial demineralization process. In order to simulate the actual oral condition, the samples were placed in a wet state during laser irradiation because the oral cavity is always filled with water vapor. To maintain the moist state, a gauze containing phosphate-buffered saline (D8537–500 ML; Sigma-Aldrich, St. Louis, MO, USA) was placed in a sealed container, and the samples were placed in the container for 10 min prior to laser irradiation. The weight ratio occupied by water contained in a sound dentin slice and a caries model was measured with using a moisture meter (MOC 603 u; Shimadzu, Kyoto, Japan). The absorption coefficients for the sound dentin slices and caries models at a wavelength of 2.94 μm were 980 and 1530 cm^{-1}, respectively [66]. The absorption coefficient of water at the same wavelength was measured by Fourier transform infrared (FTIR) spectrometry (MB3000, ABB, Switzerland). The specific gravity of dentin was 2.1 which was the ratio of the density of a substance to the density of water [67]. The volume ratio of dentin and water was calculated using the specific gravity and the weight ratio occupied by water contained in the sound dentin slice and the caries model, and then the absorption coefficients of sound dentin slices and caries models with the contained water were calculated to understand the difference in the optical absorption coefficients between sound and caries dentin.

2.2.2 Laser devices for dental treatments

The characteristics of laser ablation to dentin was evaluated with a Q-switched Er:YAG laser with a rotating mirror Q-switching system. A flash lamp–pumped Er:YAG laser (FLPM-90; Pantec Medical Laser, Liechtenstein) was attached to the Q-switched Er:YAG laser. The flash lamp–pumped Er:YAG laser, Q-switch controller, power supply unit (PS 5020; Pantec Medical Laser) to drive the flash lamp, and chiller (P 315; ThermoTek, Flower Mound, TX, USA) were connected to the laser oscillation system. A free-running Er:YAG laser (Erwin AdvErL; J. Morita Mfg., Osaka, Japan) was also used for comparison with the Q-switched Er:YAG laser in this study. Table 2.1 describes the specifications and irradiation conditions of the Q-switched Er:YAG laser and the free-running

Er:YAG laser. The wavelength was the same at 2.94 μm, but the pulse duration was different. The pulse duration of the Q-switched Er:YAG laser was 80–130 ns and that of the free-running Er:YAG laser was around 200 μs. The pulse repetition rate of the free-running Er:YAG laser was constant at 10 Hz, but that of the Q-switched Er:YAG laser was changed between 10 and 23 Hz.

Table 2.1 Irradiation conditions of Q-switched Er:YAG laser and free-running Er:YAG laser. The wavelength of the two lasers was 2.94 μm. The pulse duration of the Q-switched Er:YAG laser was 80–130 ns and that of the free-running Er:YAG laser was ~200 μs. The fluence was set to 6, 10 and 14 J/cm^2. The laser irradiation was conducted without water spray.

	Q-switched Er:YAG laser	Free-running Er:YAG laser
Wavelength	2.94 μm	
Pulse duration	80–130 ns	~200 μs
Pulse repetition rate	10–23 Hz	10 Hz
Beam area	0.36 mm^2	0.11 mm^2
Fluence	6, 10, 14 J/cm^2	
Peak power density	6.0×10^7, 10×10^7, 14×10^7 W/cm^2	4.0×10^4, 6.6×10^4, 9.2×10^4 W/cm^2
Water spray	None	

2.2.3 Irradiation setup

Figure 2.1 illustrates the optical setups for the Q-switched Er:YAG laser or the free-running Er:YAG laser. The laser beams were focused by the plano-convex lens after the output was adjusted with ND filters, and the laser was irradiated to the sound dentin slices and caries models horizontally placed on a three-axis translation stage. The stage was fixed during the laser irradiation.

The beam diameters were measured by the full width at half maximum (FWHM) of the beam profiles obtained by the knife edge method. The beam shape of the Q-switched Er:YAG laser was an elliptical with a major axis of about 700 μm and a minor axis of about 660 μm after focused using a plano-convex lens with a 100-mm focal length. The beam areas was calculated to about 0.36 mm^2 for the Q-switched Er:YAG laser. On the other hand, the beam shape of the free-running Er:YAG laser was an approximately circular. The beam diameter of the free-running Er:YAG laser was about 370 μm after focused using a plano-convex lens with a 150-mm focal length. The beam areas was calculated to about 0.11 mm^2 for the free-running Er:YAG laser. The pulse energy was also calculated from the power of laser beams measured as the actual power output from the optical setups with using a power meter (30A-P, Ophir Optronics, Israel) and a display (Nova II, Ophir

11

Optronics) and pulse repetition rate. The pulse duration was evaluated with a HgCdZnTe detector (PD-10.6.3; Boston Electronics, Brookline, MA, USA) and a digital oscilloscope (TDS3054C; Tektronix, Beaverton, OR, USA), and then the peak power was calculated from the pulse energy and pulse duration. The irradiation time was automatically set to 2 s using an electronically controlled mechanical shutter (F77; Suruga Seiki, Shizuoka, Japan). The pulse repetition rate was set to 10 Hz. The fluence was changed to 6, 10, or 14 J/cm^2, and the total applied dose was changed to 120, 200, or 280 J/cm^2. The fluence and the total applied dose were adjusted using infrared neutral-density (ND) filters with optical densities of 0.3 or 0.5 (no. 64-353, no. 64-354; Edmund Optics, Barrington, NJ, USA) to keep the laser beam diameter constant regardless of the laser oscillation output. The irradiation experiments were conducted without water spray for both lasers to compare the ablation properties under the same fluences. In addition, the power fluctuation of the two lasers were measured using the diffuse reflected light of the two lasers under 10 Hz using the HgCdZnTe detector and the digital oscilloscope.
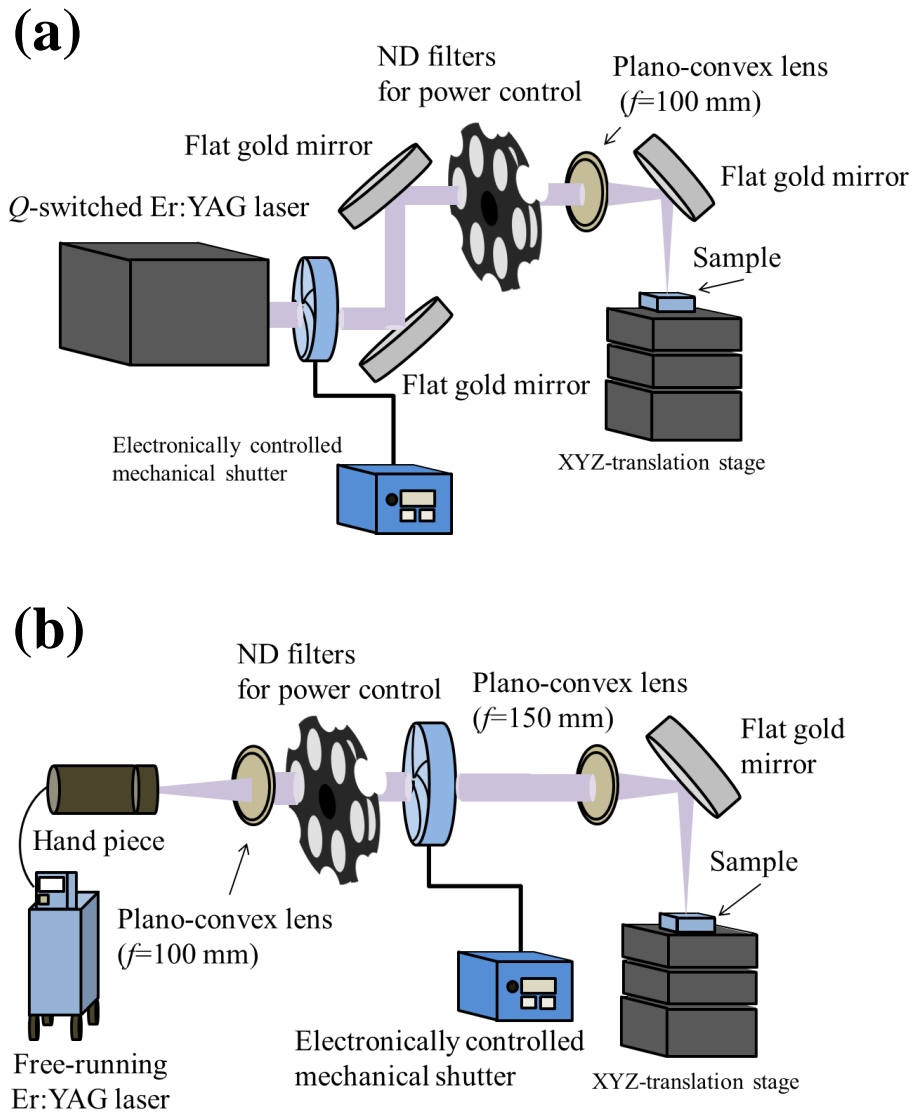
Figure 2.1 Optical setups with (a) Q-switched Er:YAG laser and (b) free-running Er:YAG laser. The laser beam was focused by a plano-convex lens after the output was adjusted with ND filters, and the laser was irradiated to the sound dentin slices and caries models horizontally placed on a three-axis translation stage.

2.3 Evaluation

2.3.1 Morphology analysis: Scanning electron microscope

A scanning electron microscope (SEM) is able to capture a sample image with third dimension as a secondary electron image and widely used in all fields such as medical and biological fields, engineering, chemistry and so on. In dentistry, it is commonly used in basic research such as observation of mark after laser irradiation and hybrid layer. SEM utilizes the properties of electrons as waves. When electrons are irradiated on a substance, various kinds of electrons and electromagnetic waves are generated by the interaction between electrons and substances. Electrons which are given the energy of incident electrons and jump out of the atomic shell are called secondary electrons. Besides, reflected electrons caused by backward elastic scattering of incident electrons and auger electrons and characteristic X-ray generated by electron transition from the excitation state to the ground state are released. Since the energy of secondary electrons emitted form atoms is small, only secondary electrons generated from a very shallow surface layer of about 10 nm can be detached from the sample surface. Therefore, an emission amount of the secondary electron rises as the inclination angle of the sample surface increases, which suggests that the emission amount of the secondary electron varies according to the undulation of the sample surface. SEM image is formed by reflecting the contrast of the secondary electron emission amount. The emission rate of the secondary electron shows not only the surface shape of the sample but also its dependence on the composition of the sample. The contrast of the emission rate of secondary electron depending on composition is called atom number effect, and atomic number is proportional to the emission rate of secondary electron in the region of small atomic number. In hard tissues, substances with small atomic numbers such as carbon, oxygen, hydrogen and nitrogen and substances with large atomic numbers such as calcium, which is peculiar to hard tissues coexist, and the contrast could be seen by the distribution of calcification degree. In this study, the laser irradiated areas were observed with a scanning electron microscope (SEM, JCM-5700; JEOL, Tokyo, Japan) to observe the dentin morphology after the laser irradiation with the two lasers. As a pretreatment before the SEM observation, the surfaces of the dentin samples were coated with 4-nm-thick gold using an ion-sputtering system (E-1010; Hitachi, Tokyo, Japan) for 30 s at a 15-mA current to prevent overcharge of the sample.

2.3.2 Measurement of ablation depth: Confocal laser microscope

In ordinary optical microscope observation, a whole area of a sample is uniformly irradiated with light, and the transmitted light or the fluorescence generated from the sample are observed. Because an image derived from a focused surface is overlapped by blurring derived from the other unfocused

surfaces when the sample has a thickness, it is difficult to observe the focal plane. Using the confocal microscope, a focused image of a surface that is an optical tomogram (sliced image) is able to be obtained by excluding light from unfocused surfaces of a sample with a pinhole. A sharp image which has a high resolution in the height direction and shallow depth of focus getting rid of blurring can be obtained. Laser light with high luminance and strong directivity is an ideal light source of a confocal microscope. In a confocal laser microscope, one point irradiation and one point detection are performed at a high speed in a wide field of view (X, Y direction) using a galvano mirror scanner, and the signal intensity of each point is imaged. Furthermore, a three-dimensional structure is able to be reproduced by combining images of multiple planes since a confocal laser microscope has high resolution in the depth direction (Z direction). In this study, the ablation volumes after laser irradiation were measured using a confocal laser-scanning microscope (OLS 3000; Olympus, Tokyo, Japan). For the measurement results, the mean with the standard deviation was shown in graphs. As a statistical process, student's t test was utilized to determine significant differences to the values compared in this study. A probability value of $p < 0.005$ was considered to indicate the statistical significance in this study.

2.3.3 Temperature measurements

In the conventional caries treatment with the free-running Er:YAG laser, water spray is necessary for cooling, which leads to the increase of the ablation efficiency as well. The irradiation energy increases the temperature of the dental pulp in a condition without water spray for cooling, which might cause necrosis of the dental pulp [68]. Generally speaking, the necrosis of dental pulp is induced when the pulp temperature increases by 5 °C or more [69, 70]. Therefore, the temperature of the pulp due increased by laser irradiation should be below 5 °C without water spray. In this study, the temperature change in the back side of the dentin sample during the Q-switched Er:YAG laser irradiation was measured for bovine sound dentin slices with a size of $5 \times 5 \times 1$ mm^3 to evaluated the acceptability of the thermal effect of the Q-switched Er:YAG laser in terms of the thermal effect on the dental pulp. A thermocouple (T35LC-200L2K98; Okazaki, Japan) was used to measure temperature. The temperature was recorded using a high-precision temperature, voltage measurement unit (NRTH08; Keyence, Osaka, Japan), and a multi-input data collection system (NR-500; Keyence). The sampling rate for the measurement was 0.1 s, and the system was heated for 30 min before the measurement. The samples were heated and kept at 37 °C to simulate the temperature of the human body using a laser mount (TCLDM 9; Thorlabs, USA) and a temperature controller (ITC4001; Thorlabs). The measurement surface of the thermocouple was in close contact with the back of the samples, and the Q-switched Er:YAG laser was irradiated on the sample surface approximately above the location of the tip of the thermocouple. The peak power density was set to 6.0×10^7 W/cm^2 and the laser irradiation time was set to 1, 2, or 4 s. The laser irradiation time was

determined by considering the actual assumed time for dentists to irradiate continuously a point on the dentin using a laser. The fluence was 6 J/cm^2 and the total applied dose was 60, 120, or 240 J/cm^2 for each irradiation time.

2.4 Results

2.4.1 Ablation depth of sound dentins and caries models

The weight ratio occupied by water in the sound dentin slice and the caries model was measured using the moisture meter, and the absorption coefficient of water at the wavelength of 2.94 μm was measured by FTIR to confirm the difference in the optical absorption coefficients between sound and caries dentin. The moisture contents contained in the sound dentin slices and the caries models were 18 % and 61 %, respectively. The absorption coefficient of water at the wavelength of 2.94 μm was 12,202 cm^{-1} according to FTIR spectrometry. Therefore, the calculated absorption coefficients of sound dentin slices and caries models were 2579 cm^{-1} and 7727 cm^{-1}, respectively, by the calculation of adding the absorption coefficient of water based on the volume ratio of dentin and water.

To improve the selectivity of caries removal with the nano-second pulsed Q-switched Er:YAG laser by reducing the thermal effect, the ablation characteristics of the Q-switched Er:YAG laser were investigated and compared with the micro-second pulsed free-running Er:YAG laser. Figure 2.2 shows the SEM images of the surface morphology of sound dentin slices and caries models after laser irradiation with the Q-switched Er:YAG laser and the free-running Er:YAG laser at the fluence of 6, 10, or 14 J/cm^2 at the pulse reputation rate of 10 Hz. The left images showed the whole irradiated areas of sound dentin slices and caries models irradiated with the two lasers, and the right images showed the enlarged images of the center parts "Center" and borders "Border" of the irradiated areas at the fluence of 10 J/cm^2. The irradiation areas with the Q-switched Er:YAG laser were larger than the free-running Er:YAG laser due to the difference in the beam area. In the enlarged images, dental pulps were observed as open after irradiation with the two lasers at the center part of the caries models. Many open dentinal tubules were observed in the image of the Q-switched Er:YAG laser. On the other hand, an uneven scale-like structure was observed at the center part of caries model irradiated with the free-running Er:YAG laser. In addition, the dentinal tubules melted at the border part of caries model due to the thermal effect, as can be seen at the border of the caries model between the irradiated and non-irradiated areas. From the morphological observation of the laser irradiation area by SEM, it was suggested that the Q-switched Er:YAG laser could suppress the thermal effect compared with the free-running Er:YAG laser.
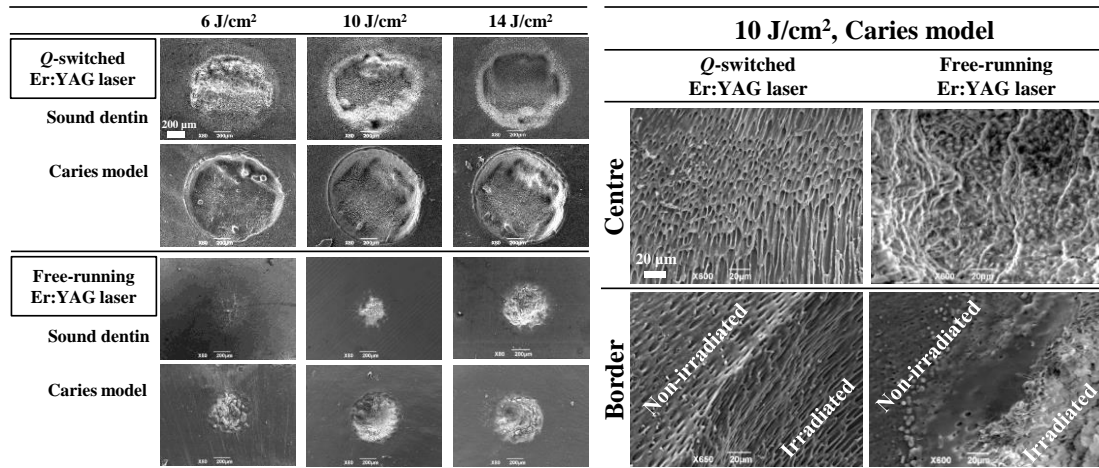
Figure 2.2 SEM images of sound dentin slices and caries models irradiated at the fluence of 6, 10, or 14 J/cm^2 at the pulse reputation rate of 10 Hz with the *Q*-switched Er:YAG laser and the free-running Er:YAG laser. The left images showed the whole irradiated areas of sound dentin slices and caries models irradiated with the two lasers, and the right images showed the enlarged images of the center parts and borders of the irradiated areas of caries models at the fluence of 10 J/cm^2.

Figure 2.3 shows the relationships between the ablation depth and irradiation conditions at the pulse reputation rate of 10 Hz of the *Q*-switched Er:YAG laser (a) and the free-running Er:YAG laser (b). Table 1.2 describes the ablation depth of sound dentins and caries models irradiated with the *Q*-switched Er:YAG laser and the free-running Er:YAG laser without water spray under the fluence of 6, 10 and 14 J/cm^2. The average and standard deviation are shown under each irradiation condition. In this study, the ratio of the volume to the beam area was introduced because the beam areas of the two lasers were different, and the ratio was defined as the ablation depth. With regard to the ablation efficiency, the ablation depths by the *Q*-switched Er:YAG laser were about three times larger than the free-running Er:YAG laser. From the perspective of selective removal for caries, according to the statistical analysis using Student's *t* test at a significance of 0.5 %, the significant difference of ablation depth between sound dentin and caries model was confirmed only at the fluence of 6 J/cm^2 for the *Q*-switched Er:YAG laser. On the other hand, the significant difference was confirmed at the fluence of 6, 10 and 14 J/cm^2 for the free-running Er:YAG laser although it is difficult to achieve the laser treatment of the free-running Er:YAG laser without water spray.
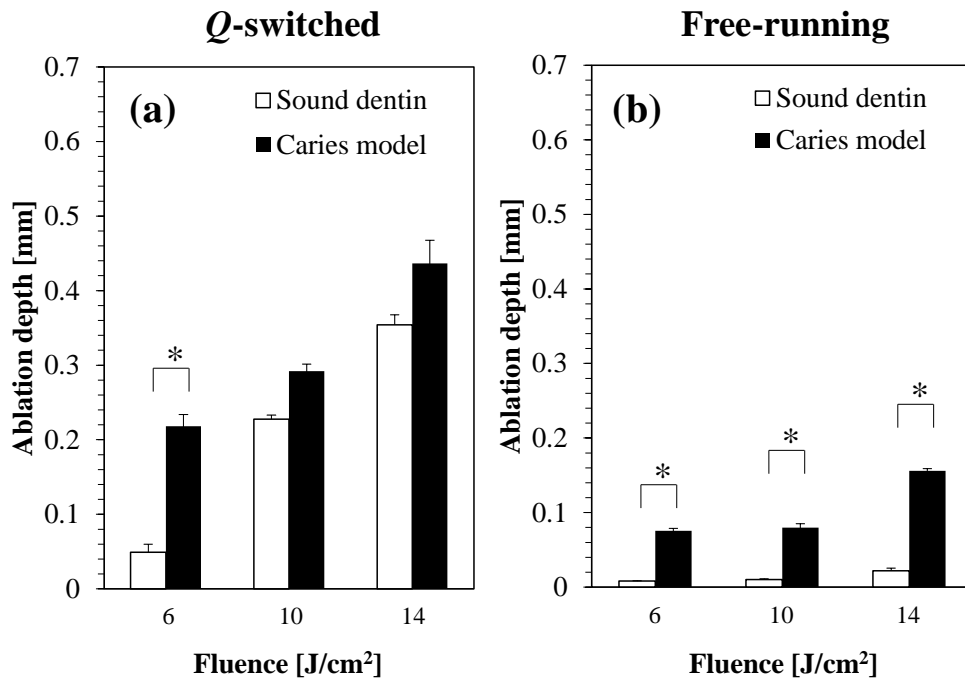
Figure 2.3 Relationships between the ablation depth and irradiation conditions at the pulse reputation rate of 10 Hz of (a) Q-switched Er:YAG laser and (b) free-running Er:YAG laser. ($n = 3$, $*p < 0.005$) For the Q-switched Er:YAG laser, the significant difference of ablation depth between sound dentin and caries model was confirmed only at the fluence of 6 J/cm^2 but for the free-running Er:YAG laser, the significant difference was confirmed at the fluence of 6, 10 and 14 J/cm^2.

Table 2.2 Ablation depth of sound dentins and caries models irradiated with the Q-switched Er:YAG laser and the free-running Er:YAG laser without water spray under the fluence of 6, 10 and 14 J/cm^2. The average and standard deviation are shown under each irradiation condition.

	Fluence [J/cm^2]		
	6	10	14
	Ablation depth [mm]		
Q-switched Er:YAG laser			
Sound dentin	0.049 ± 0.011	0.228 ± 0.005	0.354 ± 0.013
Caries model	0.218 ± 0.016	0.292 ± 0.095	0.437 ± 0.031
Free-running Er:YAG laser			
Sound dentin	0.008 ± 0.002	0.010 ± 0.001	0.022 ± 0.004
Caries model	0.076 ± 0.003	0.080 ± 0.005	0.156 ± 0.003

In Figure 2.3, the selective removal of caries models at the significance of 0.5 % with the Q-switched Er:YAG laser was observed only at the fluence of 6 J/cm^2. Here, it was hypothesized that the differences in peak power intensity might be responsible for the differences in the selectivity of caries removal because the fluences and pulse reputation rates were set to the same between the Q-switched Er:YAG laser and the free-running Er:YAG laser. Total applied doses can be adjustable by changing the pulse repetition rate of the Q-switched Er:YAG laser to 10, 16, or 23 Hz instead of changing the ND filters. When the total applied doses were changed with the pulse repetition, the peak power density can be constant. Figure 2.4 shows the ablation depth of sound dentin slices and caries models irradiated by the Q-switched Er:YAG laser and the free-running Er:YAG laser at the pulse repetition rate of 10, 16, or 23 Hz. The peak power density under all conditions was constant at 6.0×10^7 W/cm^2, which corresponds to that for the fluence of 6 J/cm^2 in Figure 2.3. In Figure 2.3, the selective ablation of the caries model was observed for the Q-switched Er:YAG laser at a probability value of $p < 0.005$ only with the peak power density of 6.0×10^7 W/cm^2. On the other hand, the selective removal of the caries model was observed at the total applied dose of 120 J/cm^2 at 10 Hz, 200 J/cm^2 at 16 Hz, or 280 J/cm^2 at 23 Hz of the Q-switched Er:YAG laser at the significance of 0.5 % as shown in Figure 2.4. The result suggested that the peak power density was the important parameter related to the selective removal of caries. In addition, the increase of ablation depth was only related to the higher number of pulses because the peak power was constant.
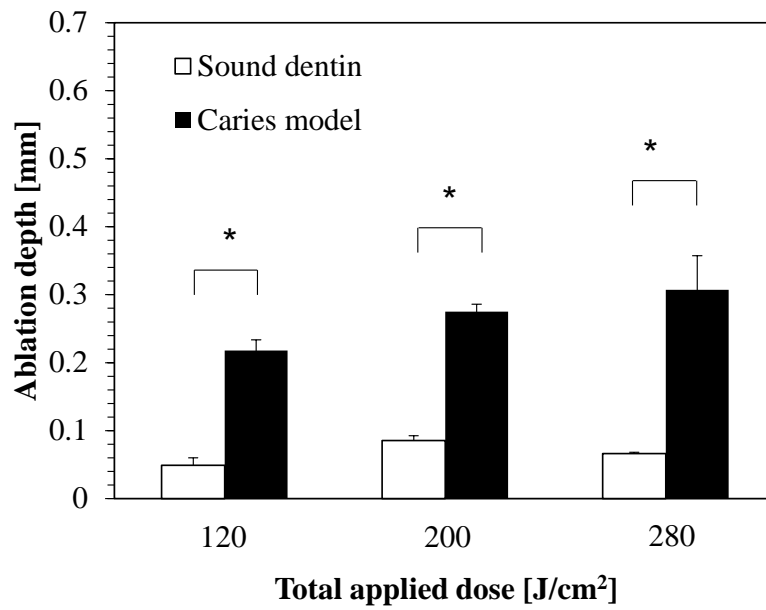
Figure 2.4 Relationships between ablation depth and the total applied dose adjusted with changing the pulse repetition rate of 10, 16, or 23 Hz using the Q-switched Er:YAG laser. (n = 3, *p < 0.005) The significant difference of ablation depth between sound dentin and caries model was confirmed at the total applied dose of 120, 200 and 280 J/cm^2.

2.4.2 Temperature measurements

The temperature change in the back of the sample during the Q-switched Er:YAG laser irradiation was measured for bovine sound dentin slices to evaluate the thermal effect with the Q-switched Er:YAG laser irradiation to the dental pulp. Figure 2.5 shows the experimental results of temperature measurement of the back in the sound dentin slice sample with the irradiation of the Q-switched Er:YAG laser at the peak power density of 6.0×10^7 W/cm^2. The peak power density was the condition where the ablation selectivity of caries was observed as shown in Figure 2.3 and 2.4. In Figure 2.5, the line and dotted lines showed the change of temperature and the error bar showed the standard deviation. The samples were heated and kept at 37 °C to simulate the temperature of the human body, and the laser was irradiated at the time of 0 s. After the beginning of the laser irradiation at the point of 0 s, the temperature started to increase for less than 10 s. The maximum temperature increase was about 2 °C at the total applied dose of 240 J/cm^2, which showed that the temperature increase in the back on the sample was below 5 °C following the laser irradiation for 1, 2, or 4 s, which had a total applied dose of 60, 120, or 240 J/cm^2, respectively. The results suggested that the temperature increase in the dental pulp due to laser irradiation with the Q-switched Er:YAG laser with the peak power density of 6.0×10^7 W/cm^2 can be suppressed to less than 5 °C and the necrosis of the pulp due to the thermal effects of the laser irradiation could be prevented.
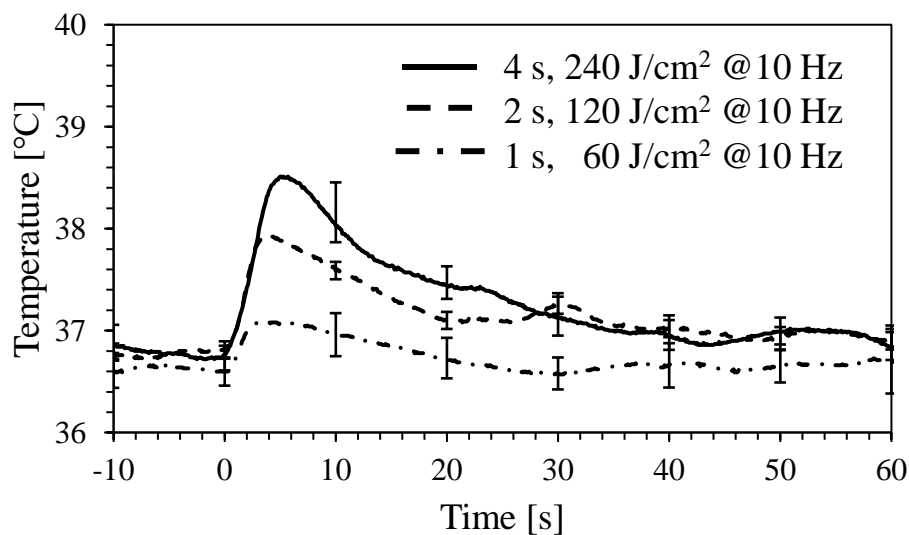
Figure 2.5 Temperatures for the back side on the sample of sound dentin slices irradiated at the total applied dose of 60, 120, 240 J/cm^2 at 10 Hz with the Q-switched Er:YAG laser ($n = 5$). The line and dotted lines showed the change of temperature and the error bar showed the standard deviation. The laser was irradiated at the time of 0 s.

2.5 Discussion

2.5.1 Ablation mechanism with the Q-switched Er:YAG laser

The ablation mechanism with the Q-switched Er:YAG laser should be discussed. In Figure 2.3, the ablation depths by the Q-switched Er:YAG laser were about three times larger than the free-running Er:YAG laser. With regard to the ablation efficiency, the Q-switched Er:YAG laser could be superior to the free-running Er:YAG laser and could be advantage to the conventional micro-second pulsed free-running Er:YAG laser. The selectivity of caries removal looked better for the free-running Er:YAG laser because the significant difference was confirmed at the fluence of 6, 10 and 14 J/cm². However, the thermal effect of the free-running Er:YAG laser was not acceptable without water spray, and in fact the dentinal tubules melted after irradiation with the free-running Er:YAG laser due to the thermal effect as confirmed in the morphological observation of the laser irradiation area with SEM.

The dentin ablation mechanisms by the two lasers might originate from two ablation processes: photothermal and photomechanical. In photothermal ablation, the temperature increase in the dentin surface can be caused when the laser reaches the boiling point of the hydroxyapatite around 3200 °C [71], or the organic matter in the dentin is evaporated and removed. On the other hand, the tissue is removed by the stress wave generated in the thermal elasticity process before the temperature increase reaches the substance's boiling point in photomechanical ablation [61]. The reaction of the separation of substances generates the stress and shock waves, which causing destruction of the hard dentin. The dominant mechanism for the ablation by the two lasers including the Q-switched Er:YAG laser and the free-running Er:YAG laser could be discussed with a stress-confinement condition. Stress confinement was established when the pulse duration was much less than the stress-relaxation time: τ_{stress}. Thus, the mechanical interaction could be used effectively, and the photomechanical ablation becomes dominant [72]. τ_{stress} was calculated as below:

$$\tau_{\text{stress}} = \frac{1}{\mu_a c_s},\tag{1}$$

where c_s was the speed of sound in a light-propagating tissue and μ_a was an absorption coefficient. The c_s values in sound and caries dentin were reported as 3.68×10^5 and 1.60×10^5 cm/s, respectively [73]. Therefore, the τ_{stress} values at the wavelength of 2.94 μm of sound and caries dentin were calculated to 2.8 and 4.0 ns, respectively. The photothermal ablation should be dominant from the consideration of the pulse durations of the two lasers. However, the pulse duration of the Q-switched Er:YAG laser was closer to τ_{stress} than that of the free-running Er:YAG laser though the stress confinement condition was not satisfied for the Q-switched Er:YAG laser. Therefore, the

23

stress diffusion was smaller and the mechanical interaction could be used more effectively.

The factor related to the selectivity of caries removal should be discussed. The selectivity of the caries model was observed at the low peak power density below 6.0×10^7 W/cm^2 as shown in Figures 2.3 and 2.4. This suggested that the peak power density might be the ablation threshold value. Two main differences could be discussed between the sound dentin slices and caries models. The difference in the absorption spectra was the first one. At the wavelength of 2.94 μm, the absorption coefficient of the sound and caries models were 2579 cm^{-1} and 7727 cm^{-1}, respectively. The caries model can absorb about three times more light than the sound dentin from the difference of absorption coefficient, which causes the ablation selectivity of caries. Mechanical strength (i.e., hardness) was the second difference. The mechanical strength of dentin was influenced by hydroxyapatite. The mechanical strength of dentin degraded by decreasing the rate of hydroxyapatite due to demineralization [74]. The Vickers hardness of sound bovine dentin and caries bovine dentin has been reported to 53.5 and 7.7, respectively [66]. The mechanical strength of caries dentin should be lower than the sound dentin, which suggests that the stress should easily reach the ablation threshold. On the other hand, the mechanical effect obtained at the low peak power density of 6.0×10^7 W/cm^2 could not be reached to the ablation threshold because the mechanical strength of the sound dentin was higher than the caries dentin. Consequently, the selective ablation was confirmed at the low peak power density.

2.5.2 Thermal effect with the *Q*-switched Er:YAG laser

In the caries treatment with Er:YAG laser, water spray is used because it induces a cavitation effect in water on dentin [57] and cooling due to the thermal effect of the laser in the treatment process, but sound dentin is also ablated, and the selectivity of the caries is sometimes poor for dental caries removal with water spray [59]. In this study, the *Q*-switched Er:YAG laser was evaluated to achieve the selective removal for caries without water spray. Figure 2.2 showed that from the morphological observation of the laser irradiation area by SEM, it was suggested that the *Q*-switched Er:YAG laser could suppress the thermal effect compared with the free-running Er:YAG laser. Non-melting of dental tissue was confirmed with the *Q*-switched Er:YAG laser satisfying the thermal confinement condition. The uneven scale-like structure observed in the irradiation area with the free-running Er:YAG laser was not observed with the *Q*-switched Er:YAG laser and the surface of dentin after the laser irradiation was smooth.

For the safely caused by the thermal effect by laser irradition, the temperature increase of the dental pulp needed to be evaluated because the temperature of the dental pulp increases in proportion to the irradiation energy without sprayed water, and the pulp becomes necrotic [68]. The necrosis of dental pulp was induced when the pulp temperature increased by 5 °C or more [69, 71]. Therefore, the temperature increase of the pulp due to laser irradiation should be below 5 °C without water

spray, and the temperature change in the back of the sample during the Q-switched Er:YAG laser irradiation was evaluated for bovine sound dentin slices. In Figure 2.5, the temperature increase in the back on the sample was below 5 °C following the laser irradiation for 1, 2, or 4 s, which had a total applied dose of 60, 120, or 240 J/cm^2, respectively. The results suggested that the temperature increase in the dental pulp due to laser irradiation with the Q-switched Er:YAG laser with the peak power density of 6.0×10^7 W/cm^2 can be suppressed to less than 5 °C and the necrosis of the pulp due to the thermal effects of the laser irradiation could be prevented. The result could be one basis for explaining the safety of the Q-switched Er:YAG laser for future clinical use.

2.5.3 Possibility of selective removal for caries with Q-switched Er:YAG laser

The characteristics of laser ablation to dentin slices were examined and compared between the Q-switched Er:YAG laser with a pulse duration of 80–130 ns and the free-running Er:YAG laser with a pulse duration of 200–300 µs without water spray to develop a less-invasive laser caries treatment using the Q-switched Er:YAG laser. In this study, caries-selective removal was observed at the low peak power density of 6.0×10^7 W/cm^2 with the Q-switched Er:YAG laser that satisfied the thermal confinement conditions. Compared to the free-running Er:YAG laser, many open dentinal tubules were observed but not an uneven scale-like structure with the Q-switched Er:YAG laser, and the Q-switched Er:YAG laser could suppress the thermal effect. In addition, the experiment for temperature measurement suggested that the temperature increase in the dental pulp due to laser irradiation can be suppressed to less than 5 °C by the Q-switched Er:YAG laser with the peak power density of 6.0×10^7 W/cm^2, and dental pulp necrosis can be suppressed without water spray.

In this study, the conditions of the Q-switched Er:YAG laser were led for the selective removal for caries, but it must be considered that the conditions were applied to the samples used in this study. Bovine sound dentin slices with a size of $10 \times 10 \times 1$ mm^3 were used as samples in this study, and caries models were prepared by immersing sound dentin slice samples into 0.1-M lactic acid solution at 37 °C while stirring for 24 h [66]. However, there are various degrees of progression of caries, and it remains unclear which irradiation conditions of the Q-switched Er:YAG laser are optimal for each progression of caries. To realize caries-selective removal with the Q-switched Er:YAG laser, laser irradiation conditions need to be determined according to the caries condition, and it is necessary for the caries conditions to be clear before the laser irradiation.

2.5.4 Relationship between selective removal for caries and dentin hardness

The selective ablation of the caries model was observed for the Q-switched Er:YAG laser with controlling the peak power density, but the condition of demineralization to create the caries model was standardized in this experiment,. However, in the clinical situation, the condition and the degree or progression of caries are various, which suggests that the optimal condition of laser irradiation for

each caries could be unclear. In the previous study, the nanosecond pulsed laser the wavelength of 5.85 µm was found to be effective for selective removal of caries dentin, and the ablation property of dentin at the wavelength of 5.85 µm was investigated based on dentin hardness [22,66,75]. The previous study showed the relationship between ablation depth and Vickers hardness of human dentin with a nanosecond pulsed laser with the wavelength of 5.85 µm at the average power density of 30 W/cm^2 for 2 seconds [22]. The caries dentins were divided into 3 types of 'Remove', 'Not remove' and 'Unclear' by the two dentists with inspection and palpation before the laser irradiation. The previous study suggested that a trend of decreasing depth of laser ablation was observed as Vickers hardness increased, which indicated that the laser ablation characteristics of dentin were dependent on hardness. In other words, the caries selective removal could be difficult to achieve in the clinical situation without the information of dentin hardness, and the information of dentin hardness is required in a clinical situation for the selective removal for caries.

2.6 Conclusion of this chapter

The purpose of the study in this chapter was to develop a less-invasive laser caries treatment using the Q-switched Er:YAG laser for achieving a caries treatment with minimal intervention. The characteristics of laser ablation to dentin slices were examined and compared between the Q-switched Er:YAG laser with the pulse duration of 80–130 ns and the free-running Er:YAG laser with the pulse duration of 200–300 µs without water spray. The suppression of thermal effect without water spray was expected with the Q-switched Er:YAG laser to achieve the selective removal for caries because the Q-switched Er:YAG laser was able to satisfy the thermal confinement condition due to the nano-second pulse duration around 100 ns. The thermal effect on the safety for dental pulp was also evaluated with temperature measurement with the laser irradiation. The ablation selectivity of the caries model was observed at the low peak power density of 6.0×10^7 W/cm^2. The ablation depths of the caries model by the Q-switched Er:YAG laser were about three times larger than those using the free-running Er:YAG laser. In addition, the Q-switched Er:YAG laser with irradiation for 1, 2, or 4 s could suppress the dental pulp necrosis because the temperature increase in the back of the sample was below 5 °C. However, the selective ablation of the caries model was observed for the Q-switched Er:YAG laser with controlling the peak power density in this study, but the condition of demineralization to create the caries model was standardized in this experiment,. In the clinical situation, the condition and the degree or progression of caries are various, which suggests that the optimal condition of laser irradiation for each caries could be unclear. In the previous study, the correlation between the laser ablation depth and the Vickers hardness, which indicated that the laser ablation characteristics of dentin were dependent on hardness. The caries selective removal could be difficult to achieve in the clinical situation without the information of dentin hardness, and the information of dentin hardness was required to understand the condition of caries before laser treatment with the selectivity of caries removal.

Chapter 3

Demonstration of an optical dentin hardness measuring device using bovine dentin with different demineralization times

3.1 Introduction

3.1.1 Significance of dentin hardness measurement

In Chapter 2, the selective ablation of the caries model was observed for the Q-switched Er:YAG laser with controlling the peak power density, but the condition of demineralization to create the caries model was standardized in this experiment. In the clinical situation, the condition and the degree or progression of caries are various, which suggested that the optimal condition of laser irradiation for each caries could be unclear and the condition of caries needed to be understood. In the previous study, the correlation between the laser ablation depth and the Vickers hardness was confirmed [22], and it was suggested that the information of detin hardness was important for the selective removal of caries. In addition, hardness testing is an indirect method to track changes in the mineral content of dentin [76,77], and the information of dentin hardness is crucial for a diagnostic perspective as well as the therapeutic perspective.

Caries, especially root caries is diagnosed by inspection and palpation. The indicators contain the color, surface texture, and hardness of the lesion [23,24]. Although the diagnosis is based on inspection and palpation, there is no clear color change in the initial root caries [25], and palpation is performed using a dental probe. Hence, the diagnosis is qualitative depending on denstists. Hardness of dentin becomes softer with the progress of caries, but the diagnosis using a dental probe depends on the dentist's sensitivity to pressure changes when inserting and removing the probe. In fact, the kappa statistics for the inspection and palpation for root caries are as low as 30 % to 51 % [26], which is very low. The quantification could improve the uncertainty of the current diagnosis of caries and might be used for definite diagnosis in cases where dentists have difficulty making

decisions. Therefore, a method to objectively and quantitatively measure the dentin hardness and evaluate the activity and progress of root caries in a clinical setting is strongly required.

3.1.2 Dentin hardness evaluation methods

The diagnosis methods such as inspection and palpation are qualitative, and a method to objectively and quantitatively measure the dentin hardness and evaluate the activity and progress of root caries in a clinical setting is strongly required. Obvious caries lesions may be seen on a simple visual clinical examination [78]. Adjunctive information or evidence of enamel roughness and softening of dentin is provided by the palpation method using an explorer or dental probe [79]. In the WHO method, lesions are classified into two stages (leathery, soft) by palpation with a community periodontal index (CPI) dental probe [80]. In addition, the International Caries Detection and Assessment System (ICDAS), which is an international caries diagnosis and assessment system, has proposed a clinical classification of the depth of the actual lesion determined using the tip of the CPI dental probe for the pathology of root caries [81]. However, the initial caries does not show a clear color change [82]. These international methods for diagnosis are also not quantitative but qualitative.

In terms of some quantitative methods for hardness evaluation, Vickers or Knoop hardness has been customarily used as an indicator of tooth hardness [83]. Both tests evaluate hardness by measuring the indentation size after pressing and removing an indenter of a quadrangular pyramid with a constant load on the target object. A drawback of these methods is that the measurement requires a dry sample because samples with a large elastic deformation like a tooth with caries does not maintain the indentation. Therefore, hardness measurements cannot be performed on an *in vivo* tooth. The tooth must be extracted prior to evaluation. Another technique to quantify the hardness of teeth in research is Cariotester. Cariotester is registered as a medical device in Japan. In this technique, paint is applie to the tip of a metal indenter and the length of the part where the paint disappears after contacting the tooth is measured [84]. Because the measurement procedure is complicated and requires a microscope for observations, this technique is difficult to utilize in clinical settings.

An objective and quantitative method to measure dentin hardness and evaluate the activity and progression of root caries in a clinical setting has yet to be established. A quantitative evaluation of hardness of *in vivo* teeth in the clinical setting may accurately evaluate the activity and progress of root caries, which may increase early detection of initial root caries and reduce the risk of becoming severe.

3.1.3 Optical dentin hardness measuring device (HAMILTOM)

In the situation that an objective and quantitative method to measure dentin hardness and evaluate the activity and progression of root caries in a clinical setting had yet to be established, an

objective and quantitative method to evaluate dentin hardness used easily in a clinical practice, a new technique and a device were proposed to easily measure the hardness of *in vivo* teeth using a light-emitting diode (LED). This technique is called "HAMILTOM," which stands for "hardness meter using indenter with light for tooth monitoring." HAMILTOM has been developed to quantify the hardness of dentin from the contact projection area (dark area) between the indenter and dentin when the indenter is pressed into the dentin by adding a load. It is expected to measure dentin hardness and evaluate the condition and progression of caries in a clinical setting, which could lead to a proper judgement for caries treatment. It should be noted that it is difficult to be used in proximal parts of teeth, but it could be used in root caries focused on this study.

3.1.4 Purpose of the study in this chapter

The objective and quantitative method to measure dentin hardness and evaluate the activity and progression of root caries in a clinical setting had been required from the perspective of realization of selective removal for caries by understanding the condition of caries and set the proper laser irradiation conditions and realization of quantitative root surface caries diagnosis. From the background, HAMILTOM has been developed as an optical dentin hardness measuring device in this study. The first purpose of this study was the demonstration of the basic principle of HAMILTOM using bovine dentin samples with different demineralization times. The dark areas and Vickers hardness were measured by HAMILTOM and a conventional Vickers hardness tester respectively, and the correlation between the dark area and the Vickers hardness was evaluated.

3.2 Materials and Methods

3.2.1 Sample preparation

The samples were twenty bovine sound dentins in the experiments of this study for the demonstration of the basic principle of HAMILTOM. Bovine dentins were used for two reasons. First, the samples were easily collected since bovine dentins are larger than human ones. Second, the samples with uniform sizes were obtained, allowing multiple points to be measured in each sample. The samples were used for the evaluation of the correlation between dark areas measured by HAMILTOM and Vickers hardness. This study was performed after the acquisition of approval from the Animal Care and Use Committee, Osaka Dental University (Approval No. 19-12001). Figure 3.1 illustrates the procedure for preparation of dentin samples from cutting, embedding to epoxy resin and cure for at least 24 hours, to mirror polishing of sample surface. As the first step, the extracted bovine tooth was cut perpendicular to the running direction of the dentinal tubules. The size of cut dentin samples were approximately $20 \times 10 \times 1$ mm^3. In order to protect the dentinal tubules from the epoxy resin solution, a manicure was applied to the back and all sides of the dentin samples prior to embedding. In the second step, the dentin samples were embedded in an epoxy resin (Crystal Resin, NISSIN RESIN, Japan) utilizing silicone molds and left to cure for at least 24 h, and then they were removed from the molds. Third, the sample surfaces were mirror polished under water injection using waterproof abrasive papers #400, 800, and 2000 (Kohnan, Japan) and a lapping film #8000 (LF1D, Thorlabs, USA) to create a horizontal hardness measurement surface. The sample tilt was adjusted to 1 deg or less during polishing for the sample orientation of 90 deg to the indenter. In addition, ultrasonic cleaning was performed for 2 minutes using a desktop ultrasonic cleaner (B2210, Branson Ultrasonic, USA) to remove the resin pieces and the inorganic components of dentin generated by polishing from the dentinal tubules. The twenty dentin samples prepared in the procedure were divided into two groups (group 1 and 2).

(a) Cutting **(b) Embedding** **(c) Mirror polishing**
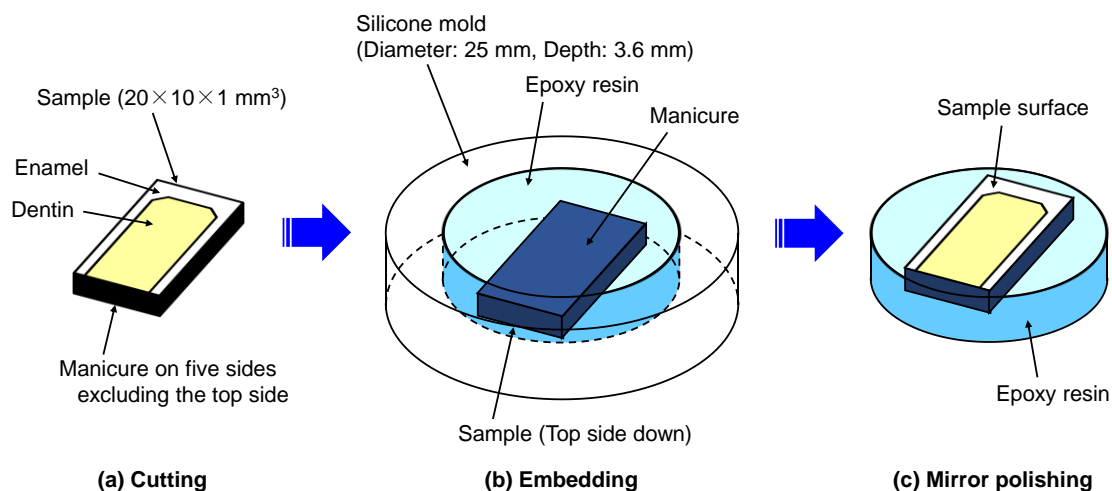
Figure 3.1 Procedures to prepare dentin samples: (a) cut the extracted bovine tooth samples to the size of approximately $20 \times 10 \times 1$ mm^3. Black manicure was Applied to the back and all sides of the dentin prior to embedding to protect the dentinal tubules from the epoxy resin solution. (b) Embed the sample in epoxy resin by using a silicone mold and let cure for at least 24 h. (c) Remove the tooth sample from the mold. The surface was and mirror polished under water injection using waterproof abrasive papers and a lapping film.

The caries models were prepared with the artificial demineralization. To create the caries models, the dentin samples were immersed in a lactic acid solution [85,86]. Lactic acid (20006-75, Nacalai Tesque, Japan) and distilled water were mixed in a beaker to prepare 1 L of 0.1M demineralization solution. The beaker was placed in a constant temperature water bath (TM-3A, AS ONE, Japan) to hold the solution temperature at 37 °C. The solution was stirred with a stirrer (HE-16GA, KPI, Japan) at the rotation speed of 1000 rpm and a pH was maintained at 2 during the demineralization process. Next, each dentin sample was immersed in the solution for a predetermined time. The demineralization time was set to 0, 0.25, 0.5, 0.75, 1, 2, 4, 6, 12, or 24 h to create caries simulated models with various hardness. After demineralization, the samples were removed from the beaker and washed with tap water and stored in saline (Otsuka Pharmaceutical, Japan) at 4 °C. For the demonstration of the basic principle of HAMILTOM, the twenty sound dentin samples were divided into two groups of ten samples each (groups 1 and 2). A group contained ten samples in which each sample was demineralized for different duration times.

3.2.2 Optical dentin hardness measuring device (HAMILTOM)

Figure 3.2 shows a schematic illustration of HAMILTOM for the demonstration of the basic principle of HAMILTOM. HAMILTOM is a device that measures the hardness of dentin from the dark area, which is the contact area between the indenter and the dentin when the indenter is pressed into the dentin by adding a load. HAMILTOM includes an optical system composed of an LED with a 455-nm center wavelength, a film diffuser (#17-682, Edmund Optics, USA), a beam splitter (#47-007, Edmund Optics), a transparent conical glass indenter with a 90-deg apex angle (#49-397, Edmund Optics), a lens with a 30-mm focal length (#45-134, Edmund Optics), and a CMOS camera (ID1MB-MDL-U, iDule, Japan) in a lens barrel. It should be noted that the coating of glass indenter was removed by immersing the indenter in hydrochloric acid before use after purchasing the glass indenter which originally had an aluminum mirror coating. The LED light passing through the film diffuser was incident on the indenter. The reflected light was reflected toward the camera by the beam splitter, and the image of the tip of the glass indenter was projected on the CMOS camera using a lens with about threefold magnification. Out of the lens barrel, a capacitive load sensor with an 8-mm diameter and 0.3-mm thickness (SingleTact S8-1N, Pressure Profile Systems (PPS), USA), a load sensor extension cable (SingleTact Tail-Extender, PPS), and an I^2C digital interface board (SingleTact Standard Electronics, PPS) were placed inside of a handpiece housing. The lens barrel rotates around the rotation axis by applying a load to the tip of the indenter, and then the lens barrel and the housing applied the load to the capacitive load sensor. The load applied to the capacitive load sensor was continuously monitored and recorded on a tablet PC (Surface Go 2, Microsoft, USA) through the I^2C digital interface board and a microcontroller (PSoC 5LP, Cypress Semiconductor, USA). An image of the indenter at the time when the load reached the set value measured by the load sensor was acquired automatically by the CMOS camera using the in-house software.
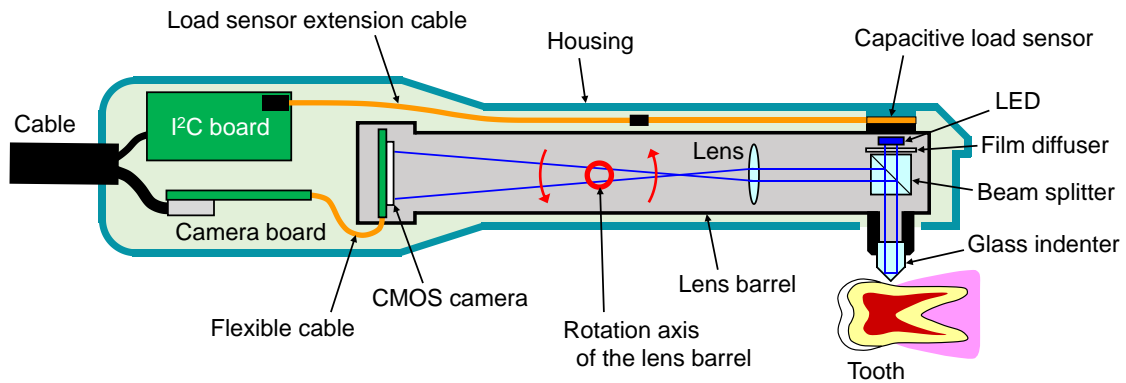
Figure 3.2 Schematic illustration of the HAMILTOM handpiece device. Image of the tip of the glass indenter was projected onto the CMOS camera with a threefold magnification using the LED light. By applying a load to the tip of the indenter, the lens barrel rotated around the rotation axis. Then the lens barrel and the housing applied the load to the load sensor. When the load reached the set value, the CMOS camera acquired an image of the indenter.

3.2.3 Measurement principle of HAMILTOM

The measurement principle of HAMILTOM is based on a total internal reflection using the differences in the refractive indexes of air, the indenter, and dentin. Figure 3.3 illustrates the measurement principle of HAMILTOM. When the indenter is not in contact with the dentin, a total internal reflection occurs at the boundary between the glass indenter and the air. Therefore, the indenter appears bright in the image of reflected light from the glass indenter taken with the CMOS camera. On the other hand, when the indenter comes into contact with the dentin, a total internal reflection does not occur. Thus, the indenter at the contact area appears dark because the refractive index of N-BK7 (1.51), which is the material of the glass indenter [87], and that of dentin (1.54) are designed to be close [88]. It is assumed that the softer the dentin, the more the dark area increases by measuring the dark area when a constant load is applied to the tip of the indenter. Therefore, the hardness of the dentin can be assessed by measuring the dark area when a constant load is applied to the tip of the indenter. Dentin becomes softer with the progressoin of caries. It is expected that the dark area indicates the degree of caries progression using the value of dark area because the dark area should increase witht the progression of caries compared to sound dentin. The physical interpretation of dark area measured by HAMILTOM has to be clarifed, but it is assumed that the dark areas are not the size of the indentation and the influence of another factor that should be the water exuded by the contact of the indenter is significant, and it is considered that the indentation might not remain after removing the indenter from dentin due to the elastic recovery of dentin.
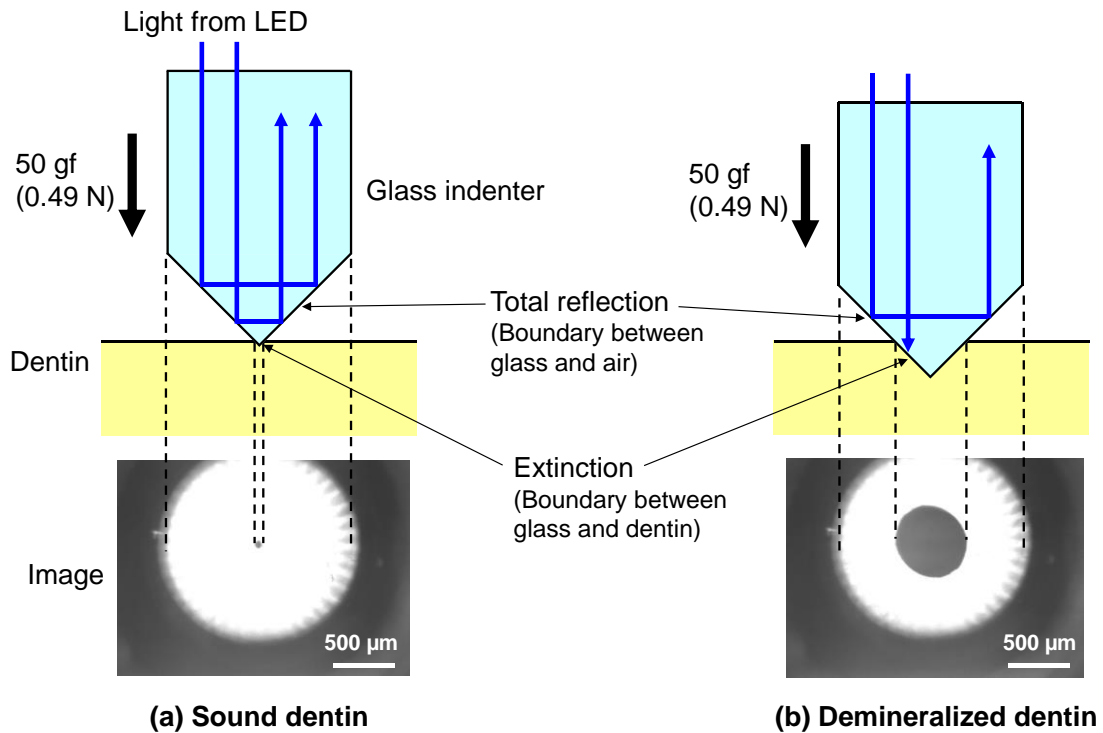
Figure 3.3 Principle of measuring the dark area projected between the glass indenter and dentin. When the indenter contacted with dentin, a total internal reflection of LED light did not occur, and the indenter at the contact area appeared dark because the refractive indices of the glass indenter and dentin were similar. (a) Dark area for sound dentin was small at a constant load of 50 gf (~0.49 N) because the sound dentin was hard. (b) The dark area for demineralized dentin is larger for the set load because the demineralized dentin was softer than sound dentin.

3.2.4 Calculation of the dark area

In this study for the demonstration of the basic principle of HAMILTOM, the dark areas were measured using HAMILTOM for the dentin samples with various demineralization time. Before each measurement, the dentin samples were immersed in saline for at least 24 hours to make them moist. Figure 3.4 shows a photograph of the experimental setup to measure the dark areas using HAMILTOM in this study. HAMILTOM was fixed with a fixed base so that the indenter tip was oriented vertically downward. The dentin sample from which the surface moisture was blown off by air was placed on a stage directly below the indenter of HAMILTOM. The threshold of the load sensor for calculation of the dark area was set to 50 gf for the demonstration of the basic principle of HAMILTOM. The stage was manually raised in the vertical direction slowly. The CMOS camera acquired an image once the load reached the specified value. For the verification of the load added to

the tip of indenter, the load was also measured by an electronic balance (ACS-5000, AS ONE, Japan) for each measurment. The accuracy of the electronic balance was confirmed before and after the experiments using a standard weight set (3-9951-04, AS ONE). Prior to the experiment, a coefficient, which was multiplied with the measured value of the load sensor, was adjusted to match the load measured with the electronic balance. After setting the dentin sample on the electronic balance, the electronic balance was reset to zero to eliminate the influence of the slight weight differences of each sample. Images of the dark area were acquired at three different positions for each dentin sample. To make it easier to find the indentation points after the first measurement, the measurement interval was standardized to 500 μm using the stage for the for the evaluation of mechanism and invasiveness of HAMILTOM. After each measurement, a lens cleaning paper (EK1546027S, Tiffen, USA) with ethanol was used for clean to remove the water and deposits on the indenter surface. In order o calculate the dark area, a reference image was obtained before the indenter was brought into contact with the sample. Once the reference image was acquired, the load measured with the load sensor was reset to zero to cancel the long-term drift of the sensor. Next, an image was acquired after the indenter was brought into contact with the sample, and then the reference was subtracted from the image. A binarized image was created with a threshold of 50 % of the maximum brightness of the subtracted image. In the binarized image, the contact area were appeared as bright pixels. Finally, the dark area was calculated from the number of bright pixels in the binarized image.
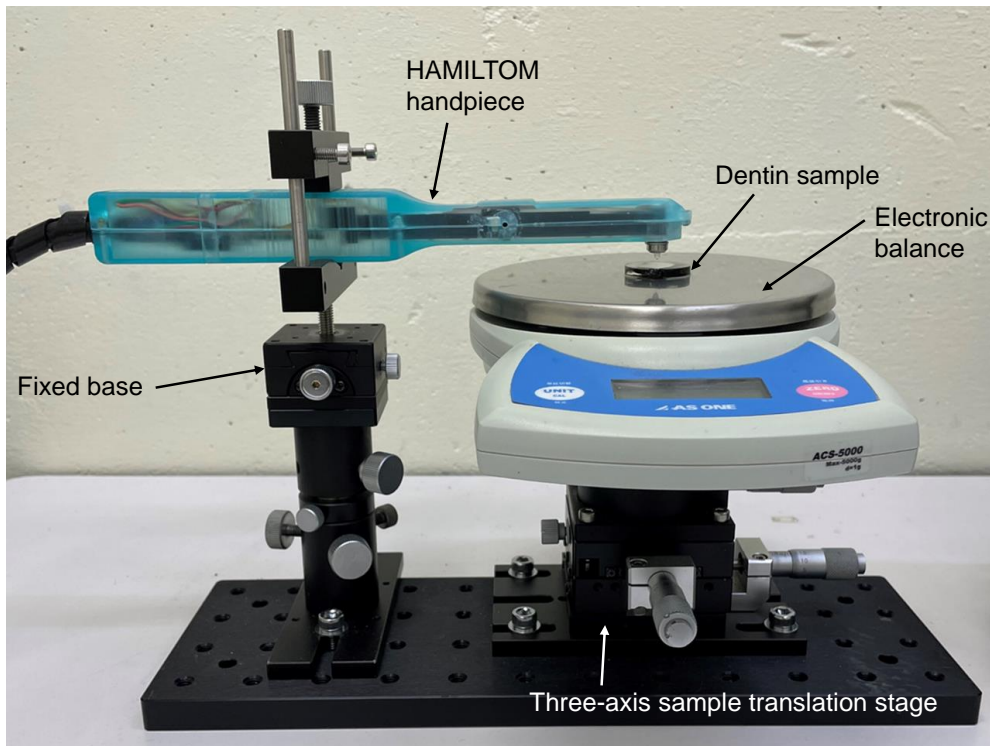
Figure 3.4 Image of the experimental system for the measurement of dark areas with HAMILTOM. HAMILTOM was fixed at the base first, and the dentin sample was located directly below the indenter of HAMILTOM. The stage was slowly raised vertically, and an image acquired with the CMOS camera when the load reaches 50 gf (~0.49 N). At the same time, the load was measured by an electronic balance to confirm the accuracy of the load measured by the load sensor.

3.3 Evaluation

3.3.1 Vickers hardness

In this study, the Vickers hardness was measured as the conventional hardness indicator. The Vickers hardness was measured using a Vickers hardness tester (HMV-G30S, Shimadzu, Japan) for each sample with different demineralization times. Conventionally, the Vickers hardness is measured in dry conditions because it is conceivable to create clear indentations on a sample in wet conditions with a large elasticity such as demineralized dentin. From the concerns, the dentin samples in this study were dried in a 23 °C indoor environment at 25 % humidity for 18 hours before the hardness measurements for the demonstration of the basic principle of HAMILTOM. In terms of the measurement conditions, the test load was set to 500 gf (~ 4.9 N), the load holding time was 10 s, and indentations were made on the dentin samples. The Vickers hardness was calculated by measuring the length of the diagonal line of the indentation by observing the indentation with the microscope of the hardness tester. The Vickers hardness of each sample was measured at three different positions in this study. The measurement points were within a 5-mm diameter with respect to the measurement points with HAMILTOM.

3.3.2 Comparison between dark area and Vickers hardness

For the demonstration of the basic principle of HAMILTOM, the correlation between dark area measured by HAMILTOM and Vickers hardness was investigated. Firstly, the dark area and the Vickers hardness of the ten dentin samples in group 1 were measured with HAMILTOM and the Vickers hardness tester, respectively. A calibration curve was created to calculate the Vickers hardness from the dark area measured with HAMILTOM from the result of group 1. After the calibration curve creation, the dark area and the Vickers hardness of the ten samples in group 2 were measured with HAMILTOM and the hardness tester, respectively with the same procedure as group 1. Finally, using the aforementioned calibration curve, the Vickers hardness were measured using both HAMILTOM and the Vickers hardness tester, and then the correlation between both methods was evaluated as the demostration of the basic principle of HAMILTOM.

3.4 Results

3.4.1 Hardness measurement of group 1

Figure 3.5 shows typical images of the reflected light from the glass indenter taken with the CMOS camera when measuring the dark areas of the samples in groups 1. Images for dentin samples with different demineralization times (0, 0.25, 0.5, 0.75, 1, 2, 4, 6, 12, or 24 h) were shown for group 1. The scale bar showed the length of 500 µm. When the dark areas were measured, the load values measured by the electronic balance were 46 to 54 gf, which suggested the load measured by the load sensor of HAMILTOM in this study had the measurement accuracy of ±4 gf. The surface quality of the glass indenter was not changed due to the repeated measurement in this study because the threshold of the load sensor was set to 50 gf and reduced the burden on the indenter. With the increase of demineralization time, the areas appearing black without a total internal reflection of the indenter increased and the shape were shown as circles. Any shape assumed as the influence of dentinal tubules were not observed in the images of the reflected light from the indenter. It is suggested that the influence of the porosity of the dentin to the dark area should be not considered.

500 µm

0 h	0.25 h	0.5 h	0.75 h	1 h
2 h	4 h	6 h	12 h	24 h

Figure 3.5 Typical images of reflected light from the glass indenter taken with the CMOS camera. Images for dentin samples with different demineralization times (0, 0.25, 0.5, 0.75, 1, 2, 4, 6, 12, or 24 h) were shown for group 1. The scale bar showed the length of 500 µm.

Table 3.1 describes the changes in the dark area and the Vickers hardness for group 1 with different demineralization times. Figure 3.6 plots the dark area, Vickers hardness, and their relationship for the samples in group 1; (a) Changes in the dark area with different demineralization times. (b) Changes in the Vickers hardness with different demineralization times. (c) Relationship between the dark area and the Vickers hardness. Dashed line showed the approximate expression. A determination coefficient was also shown for (c). Each graph showed the mean and standard deviation of three measurements.

As the demineralization time increased, the dark areas increased, but the change within 1 hour of demineralization time was smaller than the longer demineralization time. Additionally, the Vickers hardness decreased to less than half of that of the sound dentin at a demineralization time of 6 h. From the measurement results of dark area and Vickers hardness, the calibration curve was created for group 1. A power approximation as the calibration curve showed a determination coefficient of 0.96, and the correlation between the dark areas and the Vickers hardness were confirmed.

Table 3.1 Dark area and the Vickers hardness of the samples in group 1. Mean and standard deviation (SD) of three measurements with each demineralization time are shown.

		Demineralization time (h)									
		0	0.25	0.5	0.75	1	2	4	6	12	24
Dark area (mm^2)	Mean	0.0026	0.013	0.011	0.011	0.016	0.053	0.07	0.11	0.25	0.39
	SD	0.0001	0.002	0.003	0.001	0003	0.006	0.02	0.01	0.01	0.04
Vickers hardness (HV)	Mean	44	40	37	35	33	27	23	21	18	17
	SD	3	4	2	1	1	1	1	1	1	1

(a)

(b)

(c)

Figure 3.6 Dark area, Vickers hardness, and their relationship for the samples in group 1. Each graph shows the mean and standard deviation of three measurements. (a) Changes in the dark area with different demineralization times. (b) Changes in the Vickers hardness with different demineralization times. (c) Relationship between the dark area and the Vickers hardness. Dashed line showed the approximate expression. A determination coefficient was also shown for (c).

3.4.2 Hardness measurement of group 2

Figure 3.7 shows typical images of the reflected light from the glass indenter taken with the CMOS camera when measuring the dark areas of the samples in groups 2. Images for dentin samples with different demineralization times (0, 0.25, 0.5, 0.75, 1, 2, 4, 6, 12, or 24 h) were shown for group 2. The scale bar showed the length of 500 µm. When the dark areas were measured, the load values measured by the electronic balance were 46 to 54 gf, which suggested the load measured by the load sensor of HAMILTOM in this study had the measurement accuracy of ±4 gf. The surface quality of the glass indenter was not changed due to the repeated measurement in this study because the threshold of the load sensor was set to 50 gf and reduced the burden on the indenter. With the increase of demineralization time, the areas appearing black without a total internal reflection of the indenter increased and the shape were shown as circles. Any shape assumed as the influence of dentinal tubules were not observed in the images of the reflected light from the indenter. It is suggested that the influence of the porosity of the dentin to the dark area should be not considered.

Figure 3.7 Typical images of reflected light from the glass indenter taken with the CMOS camera. Images for dentin samples with different demineralization times (0, 0.25, 0.5, 0.75, 1, 2, 4, 6, 12, or 24 h) were shown for group 2. The scale bar showed the length of 500 µm.

Table 3.2 describes the changes in the dark area and the Vickers hardness for group 1 with different demineralization times. Figure 3.8 plots the dark area, Vickers hardness, and their relationship for the samples in group 2; (a) Changes in the dark area with different demineralization times. (b) Changes in the Vickers hardness with different demineralization times. (c) Relationship between the dark area and the Vickers hardness. Dashed line showed the approximate expression. A determination coefficient was also shown for (c). Each graph showed the mean and standard deviation of three measurements. As the demineralization time increased, the dark areas increased as shown in group 1. A power approximation for the relationship between the dark area and Vickers hardness showed a determination coefficient of 0.98, and the correlation between the dark areas and the Vickers hardness were confirmed in group 2.

Table 3.2 Dark area and the Vickers hardness of the samples in group 2. Mean and standard deviation (SD) of three measurements with each demineralization time are shown.

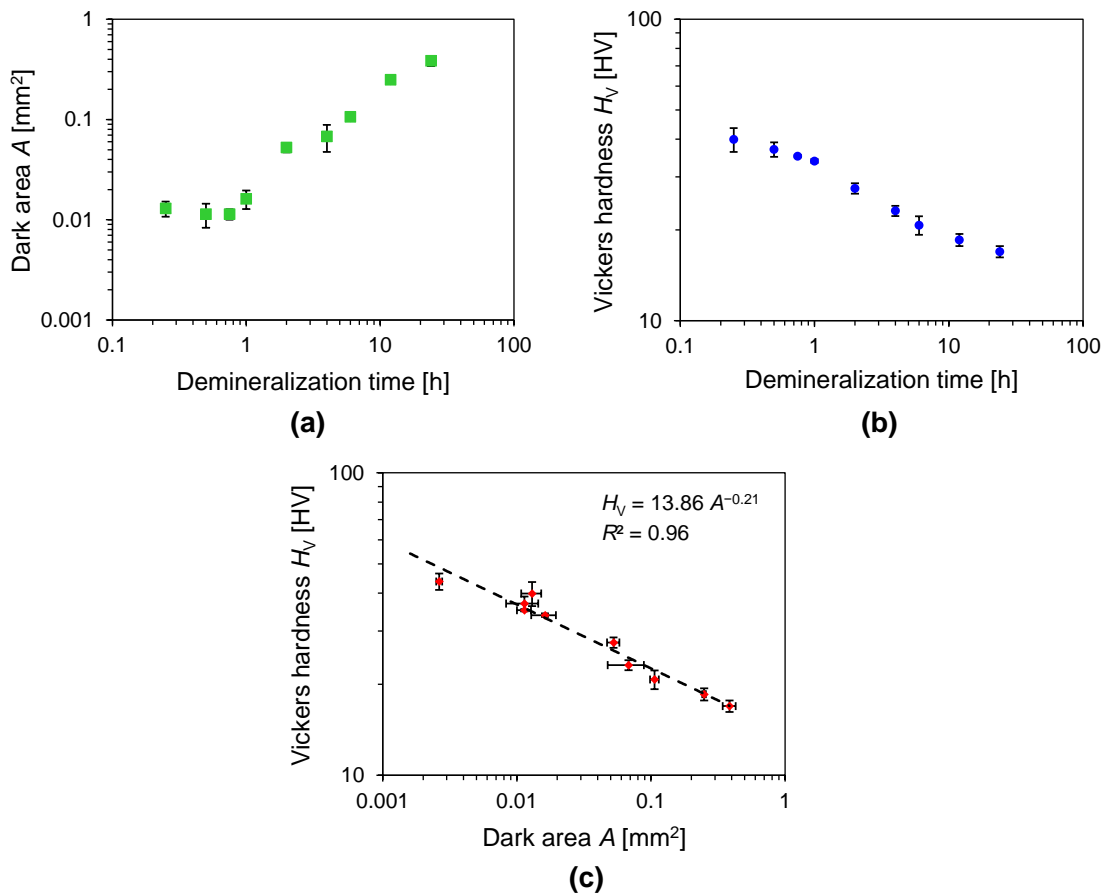|		Demineralization time (h)									
		0	0.25	0.5	0.75	1	2	4	6	12	24
Dark area (mm^2)	Mean	0.0032	0.008	0.006	0.011	0.013	0.023	0.06	0.13	0.19	0.53
	SD	0.0002	0.002	0.003	0.009	0.003	0.002	0.02	0.05	0.05	0.01
Vickers hardness (HV)	Mean	43	41	38	35	31	29	24	21	19	14
	SD	3	3	2	1	1	2	1	1	1	1
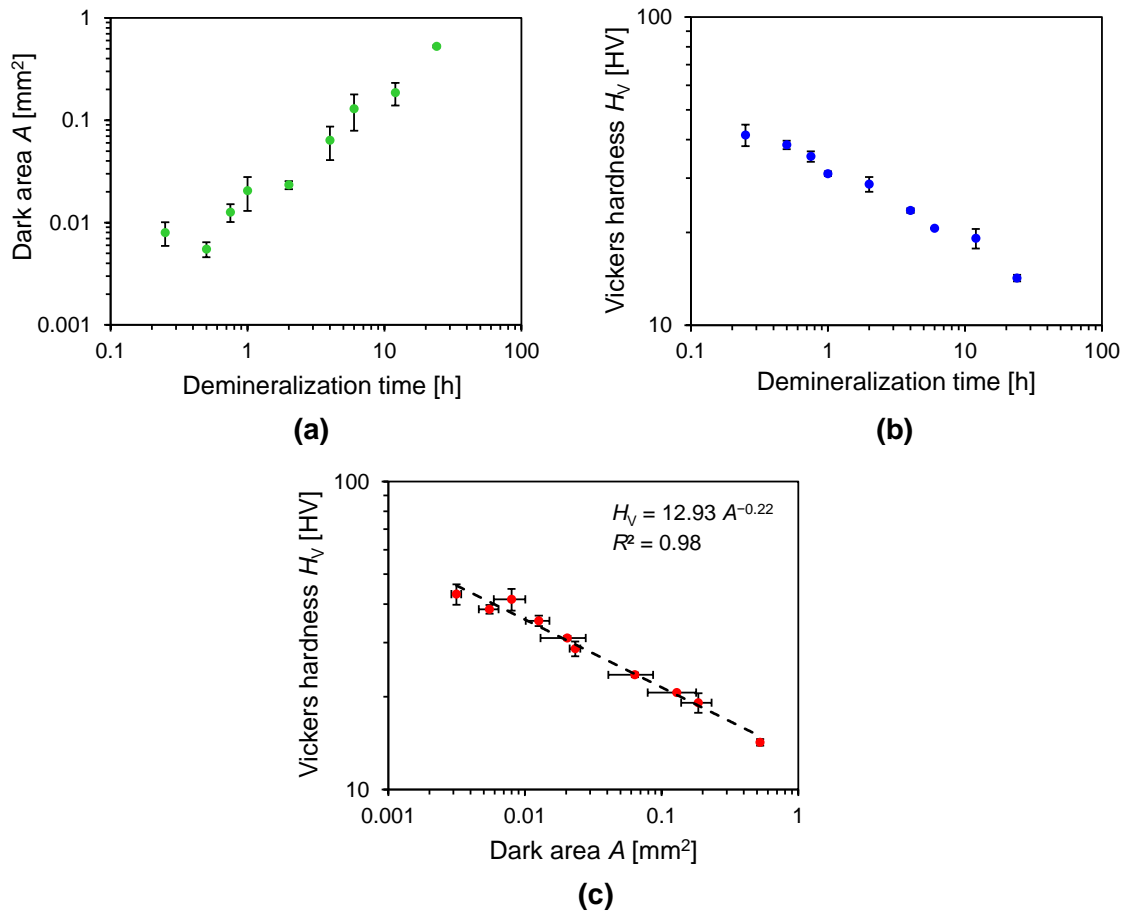
Figure 3.8 Dark area, Vickers hardness, and their relationship for the samples in group 2. Each graph showed the mean and standard deviation of three measurements. (a) Changes in the dark area with different demineralization times. (b) Changes in the Vickers hardness with different demineralization times. (c) Relationship between the dark area and the Vickers hardness. Dashed line showed the approximate expression. A determination coefficient was also shown for (c).

3.4.3 Comparison between group 1 and group 2

The dark area and the Vickers hardness of the ten dentin samples in group 1 were measured with HAMILTOM and the Vickers hardness tester, respectively, and the calibration curve was created to calculate the Vickers hardness from the dark area measured with HAMILTOM from the result of group 1. Then the dark area and the Vickers hardness of the ten samples in group 2 were measured with HAMILTOM and the hardness tester, respectively. Finally, the Vickers hardness were measured using both HAMILTOM and the Vickers hardness tester using the aforementioned calibration curve. Figure 3.9 shows the relationship between the Vickers hardness of group 2 calculated by the dark areas of group 2 and the calibration curve obtained in group 1 and the Vickers hardness of group 2 measured by the Vickers hardness tester. A strong correlation with a determination coefficient of 0.99 were shown in Figure 3.9. Furthermore, p-value of Pearson's correlation coefficient was 3×10^{-7}, and the p-value was smaller than the significance level of 5 %. Therefore, it was suggested that the correlation between the Vickers hardness measured using both HAMILTOM and the Vickers hardness tester was significant, and it was suggested that the Vickers hardness could be calculated by measuring the dark areas using HAMILTOM.
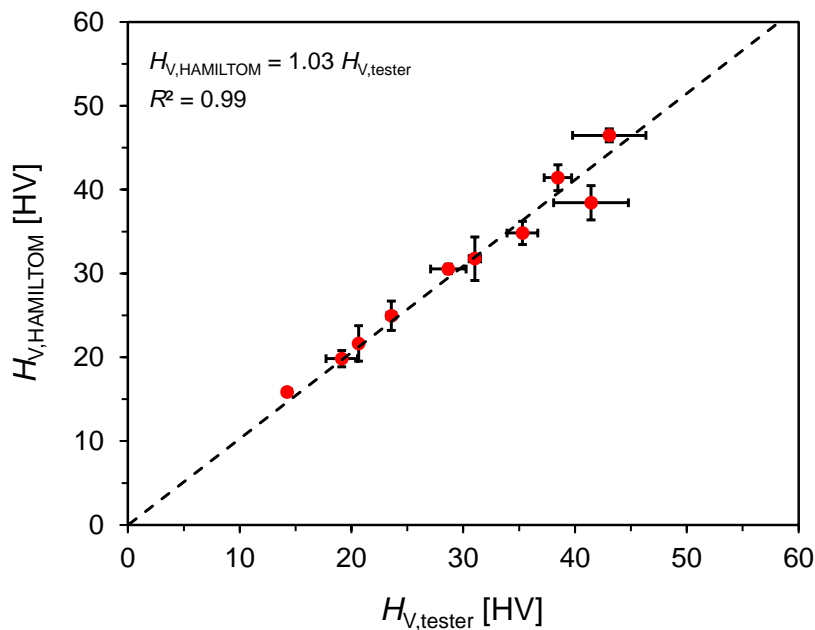
Figure 3.9 Relationship between the Vickers hardness $H_{V.tester}$ of the samples in group 2 measured with the Vickers hardness tester and the Vickers hardness $H_{V,HAMILTOM}$ calculated by the dark area of the samples in group 2 with the calibration curve obtained from the result of measurement with the samples in group 1. The mean and standard deviation of three measurements, approximate expression (dashed line), and determination coefficient were shown.

3.5 Discussion

3.5.1 Correlation between dark area and Vickers hardness

In this study, the dark areas and the Vickers hardness were measured for bovine dentins with the different demineralization times, and the correlation coefficient was evaluated. The correlation between the Vickers hardness of group 2 calculated by the dark areas of group 2 and the calibration curve obtained in group 1 and the Vickers hardness of group 2 measured by the Vickers hardness tester showed the strong determination coefficient of 0.99. Therefore, by theoretically formulating the correlation between dark areas and the Vickers hardness, it might be possible to estimate the Vickers hardness from the dark area measured using HAMILTOM. However, groups 1 and 2 had similar demineralized conditions since they were demineralized by the same procedure. In the actual caries process, various factors are included such as microbiology, saliva, tooth mineral composition, tooth ultrastructure, diffusion processes, kinetics of demineralization, the reversal of demineralization that is known as remineralization and factors that contribute to the reversal of the process [89]. The actual demineralization reaction is not driven by lactic acid, which was employed in this experiment, but is controlled mainly by bacteria such as *Streptococcus mutans* and *Lactobacillus* fermenting food and producing acid to dissolve tooth minerals [89]. It has also been reported that the origins of crown caries and root caries differ. Plaque accumulation, frequency of sugar intake, decreased saliva volume, fluoride exposure, and low standard of living are factors for both crown caries and root caries, whereas gingival recession, attachment loss, and aging also contribute to root caries [90]. Therefore, the correlation and the validity of the power approximation formula should be further evaluated to apply the power approximation formula derived in this study to actual caries of human dentins in a clinical setting. An experimental system that reproduces the actual caries process such as by a pH cycle test might be a solution to make the demineralization process more similar to the actual.

3.5.2 Measurement accuracy of HAMILTOM

The study in this chapter confirmed the correlation between the dark areas measured by HAMILTOM and the Vickers hardness measured by the Vickers hardness tester. The change in the dark areas increased significantly when the demineralization time was 2 h or more compared to the change in the Vickers hardness when the demineralization time was less than 2 h for both groups 1 and 2. The reason might be related to the measurement conditions of the dentin samples. Regarding the dark areas, the surface moisture of the dentin samples taken out from saline was blown off by air, and the measurement was performed in the wet condition. On the other hand, the Vickers hardness was measured after the dentin samples were dried in the indoor environment for 18 hours because no indentation remained due to the elastic recovery after the indenter was pulled out in the wet condition. Dentin is composed of inorganic components, collagen fibers, and water. The volume of the eluted inorganic components is replaced by water in the demineralization reaction [91]. Furthermore, the demineralized dentin is dehydrated. The unbound water between the collagen molecules is lost and the collagen fibers are aggregated by peptide bonds. The dark areas might increase as the volume of water contained in the dentin increased by the longer demineralization process. However, the change in the water content was offset by drying the dentin sample in the Vickers hardness, and the demineralized layer was condensed and showed a smaller change than the dark areas. Another reason for difference of increase of the dark areas depends on the demineralization time. Figures 3.6 and 3.8 showed that HAMILTOM might not be very sensitive within a demineralization time of 1 h, and the improvement should be studied for detection of initial caries. Due to problems with the design of the optical system, it has been confirmed that a black spot appeared at the tip of the indenter before the indenter came into contact with samples in the image of indenter taken with the CMOS camera. The size of the black spot in this experiment was 2×10^{-3} mm^2 calculated from the pixel areas. The dark areas cannot be calculated accurately when the area of the black spot exceeds the dark areas on dentin samples. Since the dark area was small in the sample with a short demineralization time, the black spot might affect the dark area easily. In order to make the area of black spot smaller than the dark area of sound dentin or initial caries, improvement to make the black spot smaller has been tried by designing the optical system and indenter. A method of suppressing the influence of black spots by increasing the threshold of the load sensor could also be possible. Since there is a trade-off relationship between invasiveness and measurement accuracy, the invasiveness might increase when the load increased and the invasiveness needs to be evaluated. It is necessary to discuss whether the current invasiveness is acceptable, but it is needed to consider whether it is possible to measure the dark area with a lower load than 50 gf by making the black spot smaller as a less invasive measurement condition.

The practical use of HAMILTOM should be realized as a method to objectively and quantitatively evaluate the activity and progress of caries, especially root caries. Hence,

HAMILTOM might support a treatment plan for caries as the diagnostic device. In particular, it might be able to determine whether the detected caries should be removed or not by quantifying the hardness of caries. The conventional Vickers hardness values of sound dentin have been reported as 50 to 60 [92] The hardness of dentin changes continuously as caries progresses. In the process, it has been reported that the area where caries dentin should be removed or preserved can be divided by a Vickers hardness of 30 to 40. Consequently, the Vickers hardness may be used as an index for caries removal [22]. Regions where the Vickers hardness was 30 or more showed small changes in the dark area in this study. The relationship between the dark area and the Vickers hardness deviates from an inverse proportional relationship in some points. To use HAMILTOM as a diagnostic device of dentin hardness and the converted Vickers hardness to determine the necessity for caries, the measurement accuracy of HAMILTOM must be improved. In this study, the average maximum error of Vickers hardness measured by the Vickers hardness tester was 5 %, whereas the average maximum error of converted Vickers hardness measured by HAMILTOM was 8 %. An error caused by the sample is considered as a common error factor, and it is possible that the hardness variation in the sample had an effect. Furthermore, a load error from 46 to 54 gf clarified by the load measurement with the electronic balance could be considered and improvement of the precision of the load is necessary to reduce a measurement error in HAMILTOM.

3.5.3 Difference of situations between *in vitro* and *in vivo*

The difference of situations between *in vitro* and *in vivo* should be discussed. In this study, the sample orientation was set to 90 deg to the indenter by adjusting the sample tilt and device orientation for the demonstration of the basic principle of HAMILTOM. However, the angle could change *in vivo* situation because the angle might depend on dentists who handle HAMILTOM in a clinical setting. In this study, it has been confirmed that the effect on the measurement accuracy was negligible when the angle of the indenter was about 5 deg to the sample surface, but the dark area is not a precise circle and expands if the angle is larger than about 5 deg to the sample surface. Therefore, a method of estimating the angle of the indenter from the circular shape and the dark area without the tilt of the indenter has been considered. In addition to the sample orientation, the surface condition of dentin and the degree and size of demineralization could be different between *in vitro* and *in vivo*. Assuming an actual clinical setting, it would be inevitable that the obtained values by HAMILTOM differ depending on the condition and size of caries. However, the current uncertainty of caries diagnosis could be improved with the qualitative inspection methods even if the influence of the condition of *in vivo* dentin is taken into consideration, and HAMILTOM might be useful in determining the need for intervention. It should be emphasized that the main purpose of HAMILTOM is to reduce the uncertainty of inspection with dentists by quantifying the degree and progress of caries as dentin hardness. The quantification could improve the uncertainty and might be

used for definite diagnosis in cases where dentists have difficulty making decisions for treatment.

3.5.4 Clinical use of HAMILTOM

The significance of the clinical of HAMILTOM should be discussed. The experimental results of dentin hardness in wet conditions using HAMILTOM suggested that the problem of the conventional hardness measuring device which can be used in dry conditions can be solved with HAMILTOM. It could be possible to measure dark areas in dry conditions as Vickers hardness measurement. However, the appeal point of HAMILTOM is that dark areas can be measured in wet conditions without removing dentins, which is superior to the Vickers hardness measurement. The Vickers hardness is measured by applying a constant load and measuring the indentation after removing the indenter. On the other hand, HAMILTOM measures the dark area while applying a load to dentins without drying. Assuming the actual practical use of HAMILTOM, the relationship between the conditions of loading time and speed and the measurement accuracy should be evaluated to clarify the influence of details of conditions of use that vary from person to person. If the hardness of root caries can be easily and quantitatively evaluated, the activity and progression of root caries can be assessed more accurately than the conventional qualitative method. The Vickers hardness is a conventional method to determine tooth hardness, but the tooth need to be removed before the measurement. Hence, it can be used for *in vivo* teeth. In contrast, HAMILTOM developed in this study can measure the dark areas in wet dentin samples. In addition, the easy hardness measurement in a clinical setting is also expected from the handpiece-type design. A study of comparison for diagnostic accuracy between HAMILTOM and classical methods, such as inspection and palpation, for root caries could be studied for clinical use in the future. HAMILTOM may realize hardness measurements of *in vivo* teeth in a clinical setting and quantitatively evaluate the occurrence and progression of dental caries by measuring the temporal change of the hardness. However, the measurement mechanism of HAMILTOM remains unclear and physically interpretation of dentin hardness measured using HAMILTOM is necessary. In addition, the invasiveness of hardness measurement with HAMILTOM needs to be clarified for the clinical use of HAMILTOM.

3.6 Conclusion of this chapter

The objective and quantitative method to measure dentin hardness and evaluate the activity and progression of root caries in a clinical setting had been required from the perspective of realization of selective removal for caries by understanding the condition of caries and set the proper laser irradiation conditions and realization of quantitative root surface caries diagnosis. From the background, HAMILTOM has been developed as an optical dentin hardness measuring device in this study. The purpose of this study was the demonstration of the basic principle of HAMILTOM using bovine dentin samples with different demineralization times. The correlation between the dark area measured by HAMILTOM and the Vickers hardness measured by the Vickers hardness tester was evaluated. As the demineralization time increases, the areas appearing black without a total internal reflection of the indenter increase. Additionally, the Vickers hardness of group 2 calculated by the dark areas of group 2 and the calibration curve obtained in group 1 and the Vickers hardness of group 2 measured by the Vickers hardness tester were strongly correlated with a determination coefficient of 0.99, which suggested that HAMILTOM might be suitable as a new device to evaluate dentin hardness in a clinical setting. The most superior point of HAMILTOM is the potential to quantitatively evaluate the progress of caries in *in vivo* teeth in wet conditions. However, the measurement mechanism of HAMILTOM remains unclear and physically interpretation of dentin hardness measured using HAMILTOM is necessary. In addition, the invasiveness of hardness measurement with HAMILTOM needs to be clarified for the clinical use of HAMILTOM.

Chapter 4

Mechanism of dentin hardness measurements using an optical dentin hardness measuring device

4.1   Introduction

4.1.1 Mechanism of dentin hardness measurements using HAMILTOM

HAMILTOM was developed as a technology that could easily and quantitatively evaluate tooth hardness using light in a clinical setting. Measurement of dentin hardness in a clinical setting is very significant because the information of dentin hardness is crucial for a diagnostic perspective for the conventional qualitative methods towards root caries as well as the therapeutic perspective for the selective removal of caries for minimal intervention. HAMILTOM quantified the hardness of dentin from the dark area between the indenter and dentin when the indenter was pressed into the dentin. The study in the chapter 3 confirmed the strong correlation between the dark areas measured by HAMILTOM and the Vickers hardness. The coefficient of determination between the Vickers hardness converted from the dark areas measured by HAMILTOM and the Vickers hardness measured by the Vickers hardness tester was 0.99, suggesting that HAMILTOM had potential to quantitatively evaluate the hardness of *in vivo* teeth. However, the measurement mechanism of HAMILTOM remains unclear and to be clarified. It is still unclear that the dark areas are not the size of the indentation and the influence of the water exuded by the contact of the indenter is significant, and it is not confirmed that the indentation does not remain due to the elastic recovery of the dentin after removing the indenter. In other words, the definition of 'Hardness' measured using HAMILTOM is unclear. Therefore, the dentin hardness measured using HAMILTOM is necessary to be interpreted physically.

4.1.2 Invasiveness to dentin using HAMILTOM

In addition to the physical interpretation of dentin hardness measured by HAMILTOM, the invasiveness of hardness measurement with HAMILTOM needs to be clarified for the clinical use of HAMILTOM because the invasiveness of palpation with a dental probe is a concern. When a dental probe is used under force, iatrogenic damage of the enamel surface may occur, promoting caries progression [78,93]. Especially, the invasiveness to sound dentin needs to be clarified because the sound dentin should be preserved without treatment after the hardness measurement using HAMILTOM. On the other hand, it might be possible that hardness measurement with the HAMILTOM is less invasive than palpation, which is more dependent on the dentist's senses, because the load during measurement is controlled with HAMITLOM. The invasiveness to dentin by HAMILTOM with those using a dental probe for palpation should be compared.

4.1.3 Purpose of the study in this chapter

The study in this chapter evaluated the mechanism of dentin hardness measurements using HAMILTOM physically and compared the invasiveness to dentin by HAMILTOM with those using a dental probe for palpation operated by a dentist. The measurement mechanism of HAMILTOM for quantitative dentin hardness evaluation had remained unclear. In addition, the invasiveness had to be evaluated to use HAMILTOM in a clinical setting because there was a concern for palpation of invasiveness with a dental probe. When a dental probe was used under force, iatrogenic damage of the enamel surface might occur, promoting caries progression [78,81]. The study in this chapter physically interpreted the dentin hardness measured using HAMILTOM and considered its measurement mechanism. Additionally, the invasiveness to dentin samples during a hardness measurement using HAMILTOM was evaluated by comparing to the invasiveness of palpation by dental probe.

4.2 Materials and Methods

4.2.1 Sample preparation

The samples were eleven bovine sound dentins in the experiments of the study of physical interpretation. Bovine dentin samples were used for two reasons. First, samples were easily collected since bovine dentin samples were larger than human ones. Second, samples with uniform sizes were obtained, allowing multiple points to be measured in each sample. Caries simulated models with various hardness were prepared with the artificial demineralization of sound dentin samples. Then the dark areas for the samples were measured with HAMILTOM. Additionally, the indentations made by HAMILTOM or a dental probe were observed using SEM (JCM-5700, JEOL, Japan). This study was performed after the acquisition of approval from the Animal Care and Use Committee, Osaka Dental University (Approval No.:19-12001).

The samples were prepared with the procedure from cutting, embedding to epoxy resin and cure for at least 24 hours, to mirror polishing of sample surface. To create caries models with different hardness, the samples were immersed in a lactic acid solution for artificial demineralization with different time for each sample [85,86]. Lactic acid (20006-75, Nacalai Tesque, Japan) and distilled water were mixed in a beaker to prepare 1 L of 0.1 M demineralization solution. The beaker was placed in a constant temperature water bath (TM-3A, AS ONE, Japan) to hold the solution temperature at 37 °C. The solution was agitated with a stirrer (HE-16GA, KPI, Japan) at a rotation speed of 600 rpm to maintain a pH of 2. Next, each dentin sample was immersed in the solution for a predetermined time of 0.25, 0.5, 0.75, 1, 2, 4, 6, 12, or 24 hours for demineralization. After the demineralization, the samples were removed from the beaker, rinsed with tap water and stored in saline (Otsuka Pharmaceutical, Japan) at 4 °C.

Nine samples were used to create the caries model with the different demineralization time, and the remaining two were stored as sound dentin samples without the demineralization process. The study in the chapter 3 employed the similar demineralization process. It was found that a demineralization time of 0–24 hours created samples with Vickers harness values of 17–44. The Vickers hardness were not measured in the study of this chapter.

The validity of the artificial demineralization by the acid etching was evaluated by measuring the actual mineral loss of the dentin samples used in this study with an energy dispersive X-ray spectrometer (JED-2300, JEOL, Japan) attached to the SEM used in this study. After the SEM observation of the indentations on the dentin samples, the dentin samples with different demineralization times were cut perpendicular to the surface in half so that the cross section of the dentin sample was exposed. Next, the surfaces of the cross section were mirror polished under water injection using waterproof abrasive papers #80, 220, 500, 1000, and 2000 (S31TO, IMT, Japan) and

4000 (S31HM, IMT, Japan). Then, the polished surfaces of the dentin samples were coated with 4-nm-thick gold using an ion-sputtering system (E-1010, Hitachi, Japan) for 30 s at a 15-mA current to prevent overcharge of the sample. The Ca content of the cross-section surface of each dentin sample was measured by element mapping, and the Ca content of the dentin sample surface where the dark areas were measured with HAMILTOM was also measured at three positions in each dentin sample. The accelerating voltage and the magnification were set to 15 kV and 300×, respectively.

4.2.2 Optical dentin hardness measuring device (HAMILTOM)

Figure 4.1 schematically illustrates the HAMILTOM handpiece used in this study. The dark area can be measured by contacting an indenter of HAMILTOM to dentin. HAMILTOM used in this study included an optical system composed of an LED with a 455-nm center wavelength, a film diffuser (#17-682, Edmund Optics, USA), a beam splitter (#47-007, Edmund Optics), a transparent conical indenter with a 90° apex angle, a lens with a 30-mm focal length (#45-134, Edmund Optics), and a CMOS camera (ID1MB-MDL-U, iDule, Japan) in the lens barrel. It should be noted that the indenter was composed of a photocuring resin and has a refractive index of 1.54 instead of the glass indenter used in the chapter 3. The glass indenter used in the study in the chapter 3 was changed into a transparent conical indenter with a 90° apex angle composed of the photocuring resin for the mass production of HAMILTOM because it was assumed that the indenters of HAMILTOM could be single use to maintain the cleanness of indenters in a clinical setting. The LED light passing through the film diffuser was incident on the indenter. A beam splitter reflected light toward the camera, and the image of the indenter tip was projected on the CMOS camera using a lens with about 1.5-fold magnification. From the lens barrel, a capacitive load sensor with an 8-mm diameter and 0.3-mm thickness (SingleTact S8-1N, Pressure Profile Systems (PPS), USA) and in-house control boards were placed in a handpiece-type polycarbonate housing. The reference acquisition button was used to obtain a reference image before the indenter was brought into contact with the sample. By applying a load to the indenter tip, the lens barrel rotated around the rotation axis. Then the lens barrel and the housing applied the load to the load sensor. The applied load to the sensor was continuously monitored on a tablet PC (Surface Go 2, Microsoft, USA) through the control boards with a USB interface. Then the CMOS camera automatically acquired an image of the indenter using in-house software at the time when the load reached a predetermined value.

The measurement principle of HAMILTOM was based on a total internal reflection using the differences in the refractive indexes of air, the indenter, and dentin. When the indenter was not in contact with the dentin, the indenter appeared bright because a total internal reflection occurred at the boundary between the indenter and the air. On the other hand, a total internal reflection did not occur when the indenter came in contact with the dentin because the refractive indexes of the indenter and dentin were designed to be close. For a constant contact load, a softer dentin should

yield a larger dark area. Dentin became softer with the progress of caries, and therefore the dark area indicated the degree of caries progression.
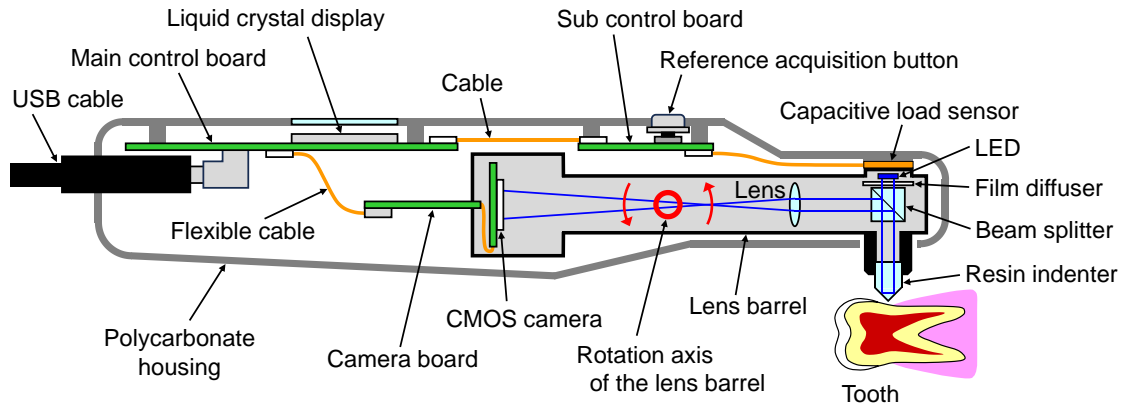

Figure 4.1 Schematic illustration of the HAMILTOM handpiece used in this study. Image of the resin indenter tip was projected onto the CMOS camera with a threefold magnification using LED light. First, the reference image was obtained by pressing the reference acquisition button. By applying a load to the indenter tip, the lens barrel rotates around the rotation axis, and the lens barrel and the housing apply a load to the capacitive load sensor. Then CMOS acquires an image of the indenter when the load reaches a predetermined value.

4.2.3 Calculation of the dark area

The dark areas were measured using HAMILTOM for the dentin sample at each demineralization time. Prior to each measurement, the dentin samples were immersed in saline for at least 24 hours to maintein the wet condition of the samples . Figure 4.2 shows a photograph of the experimental setup to measure the dark areas using HAMILTOM. HAMILTOM was fixed with a fixed base so that the indenter tip was oriented vertically downward. The dentin sample was placed on a stage directly below the indenter after blowing off the excess surface moisture with air. The threshold of the load sensor when calculating the dark area was set to 50 gf basically, but the load was changed to 10, 30, 50, 100, 150, 200, or 250 gf for the evaluation of mechanism and invasiveness of HAMILTOM to evaluate the influence of the load on the indentation created on surface of samples. The stage was manually raised in the vertical direction. The CMOS camera acquired an image once the load reached the specified value, and during the measurement, the load was measured by an electronic balance (ACS-5000, AS ONE, Japan) to verify the load accuracy. Additionaly, the accuracy of the electronic balance was verified before and after the experiments with a standard weight set (3-9951-04, AS ONE). Before the experiment, a coefficient, which was multiplied with the measured

value of the load sensor, was adjusted to match the load measured with the electronic balance. After setting the dentin sample on the electronic balance, the electronic balance was reset to zero to eliminate the influence of the slight weight differences of each sample. Images of the dark area were acquired at three different positions for each dentin sample. To make it easier to find the indentation points after the first measurement, the measurement interval was standardized to 500 μm using the stage for the for the evaluation of mechanism and invasiveness of HAMILTOM. After each measurement, a lens cleaning paper (EK1546027S, Tiffen, USA) with ethanol was used to remove the water and deposits on the indenter surface which might influence on the dark area.

In order to calculate the dark area, a reference image was obtained before the indenter was brought into contact with the sample. Once the reference image was acquired, the load measured with the load sensor was reset to zero to cancel the long-term drift of the sensor. Next, an image was acquired after the indenter was brought into contact with the sample, and then the reference was subtracted. A binarized image was created using a threshold of 50 % of the maximum brightness of the subtracted image. In the binarized image, the contact area appeared as bright pixels. Finally, the dark area was calculated from the number of bright pixels in the binarized image.
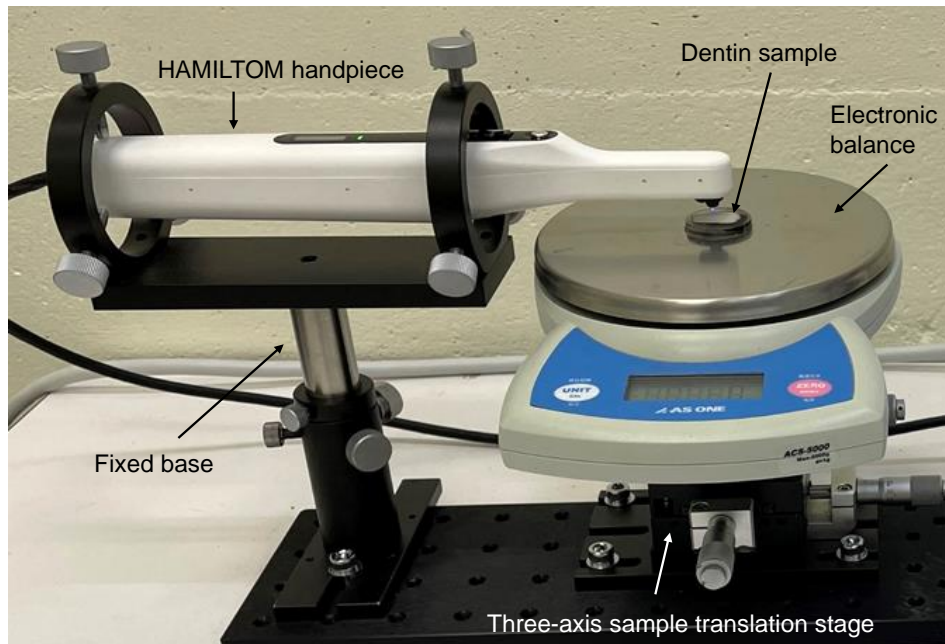
Figure 4.2 Image of the experimental system to measure dark areas by HAMILTOM used in this study. HAMILTOM was fixed at the base with the two points, and the dentin sample was placed directly below the indenter. When the dark area was measured, the stage was slowly raised vertically, and an image was acquired with the CMOS camera when the load reaches 50 gf (~0.49 N). To verify the accuracy of the load measured by the sensor, the load was also measured by an electronic balance.

4.2.4 Theoretical formula of HAMILTOM

From the relationship between the elastic modulus and the projected area of indenter/material contact based on indenter mechanics, a theoretical formula for the dark area of HAMILTOM is calculated. The indenter/material projected area generated when an indenter presses into an isotropic material is theoretically derived based on indenter mechanics. First, the indenter/material contact projected area A_e and the elastic modulus of the material when the material is perfectly elastic are linked. When the load transmitted from the indenter to the material is F and the composite elastic modulus is E_r, the Meyer hardness H_M, which represents the mechanical properties of the material, is expressed by the following formula [94]:

$$H_M = \frac{F}{A_e} = \varepsilon_I E_r \, , \qquad (1)$$

where ε_I is the indentation strain, expressed as $\varepsilon_I = (\tan\beta)/2$ using the conical indenter face tilt angle β [94]. E_r is a parameter converted by considering the elastic modulus of the indenter and material and Poisson's ratio. Next, the indenter/material contact projected area A_p and the yield stress of the material when the material is perfectly plastic is linked. H_M is expressed by the following equation using the indenter/material contact projected area A_p and the yield stress Y of the material [94]:

$$H_M = \frac{F}{A_p} = cY \, , \qquad (2)$$

where c is a constraint factor that depends on the indenter shape and the coefficient of friction between the indenter and the material. In highly plastic materials, the plastic deformation of the indenter press fit can cause pile-up, which is spillage of the plastic deformation onto the free surface of the material. c quantitatively describes the in-plane constraint on the pile-up and is given by $2.5 \leq c \leq 3.5$. Yield stress Y is the pressure at which the material will not return to its original position when the strain is increased [94]. The indenter/material contact projected area A_{proj} for an elastoplastic material with elastic modulus E_r and yield stress Y is derived. Here, the theory of excluded volume additivity, which links the increase in material free energy to the volume of material excluded by the indentation is introduced. The incremental free energy δG associated with the indenter press-in is expressed by the following equation using the mean contact pressure p_m that occurs below the indenter during the press-in [94]:

$$\delta G = p_m \delta V = p_m \delta V_e + p_m \delta V_p \, , \qquad (3)$$

where δV is the increment in excluded volume of the material induced by a small increase in mean contact pressure, and δV_e and δV_p are the increments in excluded volume related to elastic and plastic deformation, respectively. $p_m \delta V_e$ represents the incremental elastic energy and $p_m \delta V_p$ the energy dissipation due to plastic deformation. Therefore, $V = V_e + V_p$ holds. The relationship

58

between the excluded volume V and the projected area of indenter/material contact A_{proj} in a conical indenter is expressed geometrically as $V = \left((\tan\beta)/3\sqrt{\pi}\right) \cdot A_{\text{proj}}^{3/2}$. This leads to $A_{\text{proj}}^{3/2} = A_{\text{e}}^{3/2} + A_{\text{p}}^{3/2}$, where A_{e} and A_{p} represent the projected area of indenter/material contact when the same indenter is pressed into a perfect elastic material with elastic modulus E_{r} and a perfect plastic material with yield stress Y under the same load F respectively. Therefore, $A_{\text{e}} = P/\varepsilon_{\text{I}}E_{\text{r}}$ and $A_{\text{p}} = P/cY$ are shown respectively, and A_{proj} is expressed by the following equation:

$$A_{\text{proj}} = F\left\{\left(\frac{1}{\varepsilon_{\text{I}}E_{\text{r}}}\right)^{\frac{3}{2}} + \left(\frac{1}{cY}\right)^{\frac{3}{2}}\right\}^{\frac{2}{3}}, \qquad (4)$$

where an elastoplastic parameter expressed as $P = A_{\text{p}}/A_{\text{e}} = \varepsilon_{\text{I}}E_{\text{r}}/cY$ is introduced [94]. P represents the ratio of plastic deformation to elastic deformation induced within the elastoplastic body by indentation. This leads A_{proj} to be expressed from the material properties of the dentin sample of E_{r} and P shown in the following equation:

$$A_{\text{proj}} = \frac{F\left(1 + P^{\frac{3}{2}}\right)^{\frac{2}{3}}}{\varepsilon_{\text{I}} \quad E_{\text{r}}}, \qquad (5)$$

where the elastic modulus and yield stress of dentin were assumed to change at the same rate due to demineralization, and P was set to a constant. The mathematical model was also based on the study of Li et al. assuming a sound dentin with a yield stress of 75 MPa and an elastic modulus of 4 GPa in the wet state at the time of the measurements in this study [95]. Since the dark area A_{T} of HAMILTOM is the projected area of indenter/material contact during indenter indentation, $A_{\text{T}} = A_{\text{proj}}$. This leads that A_{T} can be expressed by the following equation:

$$A_{\text{T}} = A_{\text{proj}} = \frac{F\left(1 + P_{\text{A}}^{\frac{3}{2}}\right)^{\frac{2}{3}}}{\varepsilon_{\text{I}} \quad E_{\text{A}}}, \qquad (6)$$

where E_{A} and P_{A} represent the composite elastic modulus and elastoplastic parameters of the dentin sample in the measurement of the reduced light area, respectively.

4.2.5 Theoretical formula of Vickers hardness

The Vickers hardness was measured using a Vickers hardness tester (HMV-G30S, Shimadzu, Japan) for each sample, which had different demineralization times. Conventionally, the Vickers hardness is measured in dry conditions because indentations do not clearly remain on a sample with a large elasticity such as demineralized dentin. The dentin samples in this study were dried in a 23 °C indoor environment at 25 % humidity for 18 hours before the hardness measurements for the demonstration of the basic principle of HAMILTOM. The test load was set to 500 gf (~ 4.9 N). The load holding time was 10 s, and indentations were made on the dentin samples. The Vickers hardness was calculated by measuring the length of the diagonal line of the indentation. The indentation was observed with the microscope of the hardness tester. The Vickers hardness of each sample was measured at three different positions. The measurement points were within a 5-mm diameter with respect to the measurement points with HAMILTOM.

Vickers hardness H_v is an index using the surface area A_c of the indentation after indenter unloading. In the derivation of the theoretical equation, the elastic recovery after unloading was ignored and the surface area of the indentation was assumed to be equivalent to the indenter/material contact area. The behavior of the material surface during Vickers indentation can be assumed to be equivalent to that of a conical indenter with a face tilt angle of 19.7 deg. due to the excluded volume identity. Exclusion volume identity refers to the relationship that the indenter exclusion volume is equal when indenting to the same depth [94]. This assumption can avoid the complex stress distribution that occurs near the ridge of the Vickers indenter and allows the indenter/material contact projected area A_{proj} to be determined. The relationship between A_c and the indenter/material contact projected area A_{proj} is expressed geometrically as $A_c = 1.078 A_{proj}$. This leads H_v expressed by the following equation:

$$H_V = 0.102 \frac{F}{A_c} = 0.017 \frac{E_v}{\left(1 + P_v^{\frac{3}{2}}\right)^{\frac{2}{3}}} = 0.464 \frac{1}{A_{proj}}, \tag{7}$$

where E_v and P_v represent the composite modulus and elastoplastic parameters of the dentin sample in the Vickers hardness test, respectively.

4.2.6 Probe for palpation

The invasiveness to dentin samples during a hardness measurement using HAMILTOM was evaluated by measuring indentation depth and compared with palpation by a dental probe. Figure 4.3 shows a photograph of the experiment to create indentations with a dental probe by a dentist. Indentations of the dental probe (AD1 #5, YDM, Japan) based on palpation by the dentist belonging to Osaka Dental University were created at three random positions for each sound dentin sample. To moisten the dentin sample, it was immersed in saline for at least 24 hours before the experiment. Then the excess surface moisture was blown off with air prior to indentation creation. The dentist applied the same force as a clinical setting to create clinically simulated indentations on the dentin sample surface using the dental probe. In actual clinical palpation, the probe is contacted with dentin and then slid a few millimeters to check dentin hardness. Therefore, the same probing operation with a long scratch was used in this study.
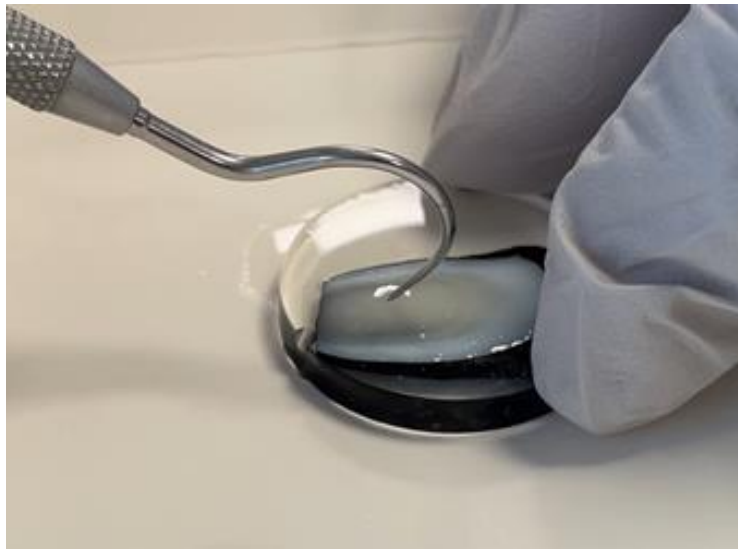

Figure 4.3 Image of the experiment to create indentations with a dental probe by a dentist. To moisten the dentin sample, it was immersed in saline for at least 24 hours before the experiment. Then the excess surface moisture was blown off with air prior to indentation creation. The dentist applied the same force as a clinical setting to create indentations on the dentin surface using a dental probe and created the indentations at three random positions for each sample.

4.3 Evaluation

4.3.1 Morphology analysis: Scanning electron microscope

SEM is able to capture a sample image with third dimension as a secondary electron image. For the evaluation of mechanism and invasiveness of HAMILTOM, the indentations made by HAMILTOM or the dental prove were observed using a scanning electron microscope (SEM, JCM-5700, JEOL, Japan). Also, the indentation area of HAMILTOM was calculated as an oval shape by measuring the long and short outer diameters of the indentation from the SEM images. Before the SEM observation, the scale bar accuracy was confirmed using a nickel mesh (EM-fine grid F-400 mesh, Nisshin-EM, Japan) to verify the reliability of scale bar. The size of one mesh square was 63.5 μm, which was the same as that measured by the SEM scale bar.

4.3.2 Measurement of ablation depth: Confocal laser microscope

Using the confocal microscope, a sharp image which has a high resolution in the height direction and shallow depth of focus getting rid of blurring can be obtained. A three-dimensional structure is able to be reproduced by combining images of multiple planes since a confocal laser microscope has high resolution in the depth direction (Z direction). In this study for the evaluation of invasiveness of dentin hardness measurement using HAMILTOM, the indentation depths created by HAMILTOM or dental probe were measured using a confocal laser-scanning microscope (OPTELICS HYBRID, Lasertec, Japan).

4.4　Results

4.4.1　Change of Ca content by artificial demineralization

　　Figure 4.4 shows the SEM images and the mapping of Ca content of the cross-section surface of each dentin sample with the different demineralization time measured with the energy dispersive X-ray spectrometer attached to the SEM used in this study. The top side of the images illustrates the dentin sample surface on which the indentations were created in this study. A gradual decrease in the Ca content was observed from the dentin sample surface with increasing demineralization time. Figure 4.5 shows the Ca content of the dentin sample surface, where the dark areas were measured with HAMILTOM, at three positions in each dentin sample with the different demineralization time measured with the energy dispersive X-ray spectrometer attached to the SEM used in this study. A clear difference in Ca content was observed between sound and demineralized dentin. The variation in Ca content with 0.25–2 hours of demineralization time was large, but as the demineralization time increased, the Ca content on the dentin sample surface decreased, ranging from 1–2% at the demineralization time of 12 hours or longer. From the observation of the change of Ca content in each dentin sample with the different demineralization time, the validity of the artificial demineralization by the acid etching in this study was confirmed.
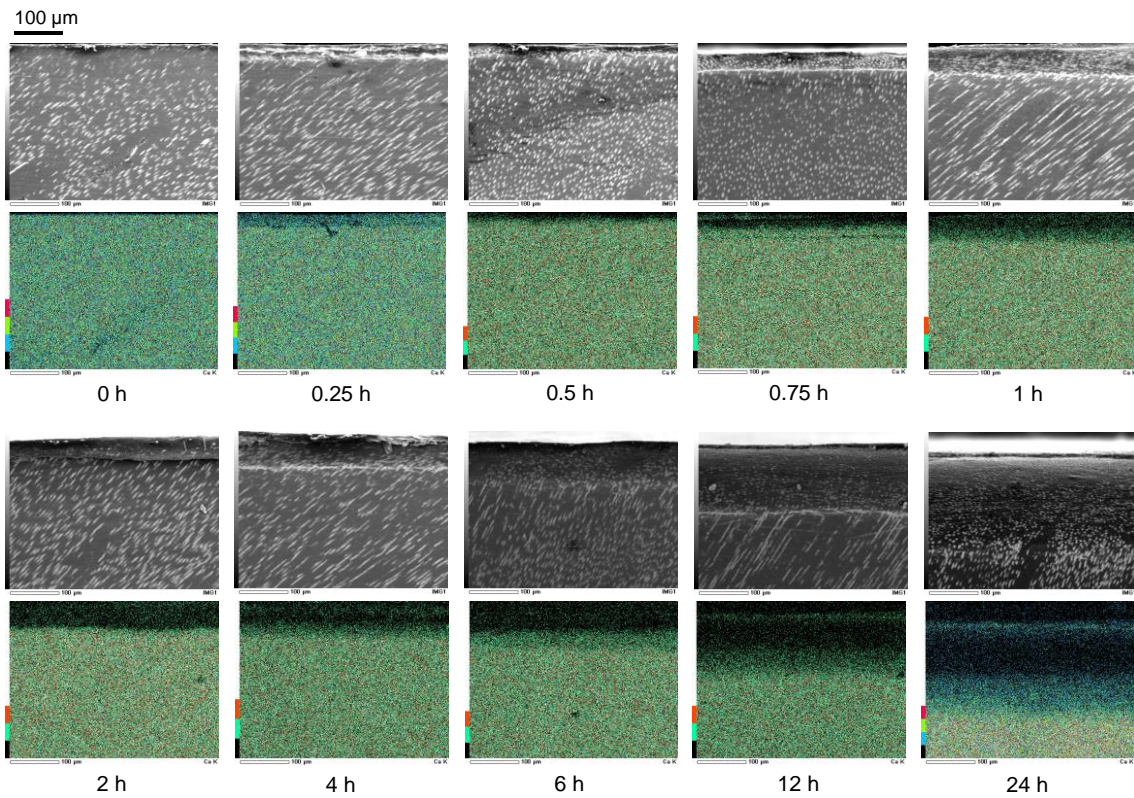
Fig. 4.4 SEM images and mapping of Ca content of the cross-section surface of each dentin sample with the different demineralization time (0.25, 0.5, 0.75, 1, 2, 4, 6, 12, or 24 h) measured with the energy dispersive X-ray spectrometer attached to the SEM used in this study. The top side of the images illustrates the dentin sample surface on which the indentations were created in this study.
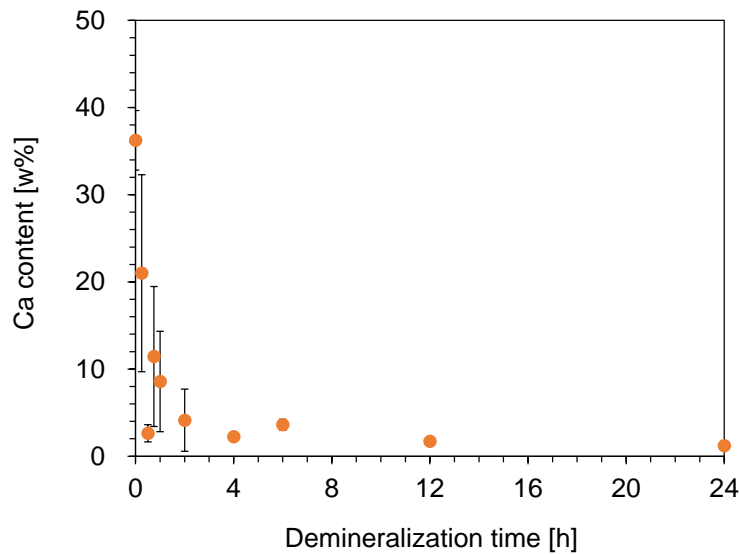
Fig. 4.5 Ca content of the dentin sample surface, where the dark areas were measured with HAMILTOM, at three positions in each dentin sample with the different demineralization time (0.25, 0.5, 0.75, 1, 2, 4, 6, 12, or 24 h) measured with the energy dispersive X-ray spectrometer attached to the SEM used in this study.

4.4.2　Dark area and indentation area

In this study, the dark area and indentation area were measured and compared to interpret the dentin hardness measured with HAMILTOM physically. Figure 4.6 shows the changes in the dark area measured using HAMILTOM with the load of 50 gf with different demineralization time. The size of the dark area measured by HAMILTOM increased with demineralization time. The dark areas with demineralization time more than 1 h increased significantly compared with less than 1 h. Table 4.1 shows dark area and the Vickers hardness of the dentin samples calculated with the calibration curve obtained in group 1. The Vickers hardness was 20–52 with the demineralization time of 0–24 hours. Figure 4.7 shows SEM images of the indentation with different Vickers hardness left on the dentin sample surface after the measurement of dark areas using HAMILTOM. The indentations were observed under all demineralization time conditions. The indentation area increased with demineralization time, but the indentation shape was indistinct for demineralization times longer than 4 hours. In the sound dentin sample without demineralization treatment, dentinal tubules in the indentation were closed and there was a crack at the center part of the indentation observed in the SEM image, whereas the dentinal tubules in the indentation in demineralized dentin samples were open and no crack was observed at the center part of the indentation.
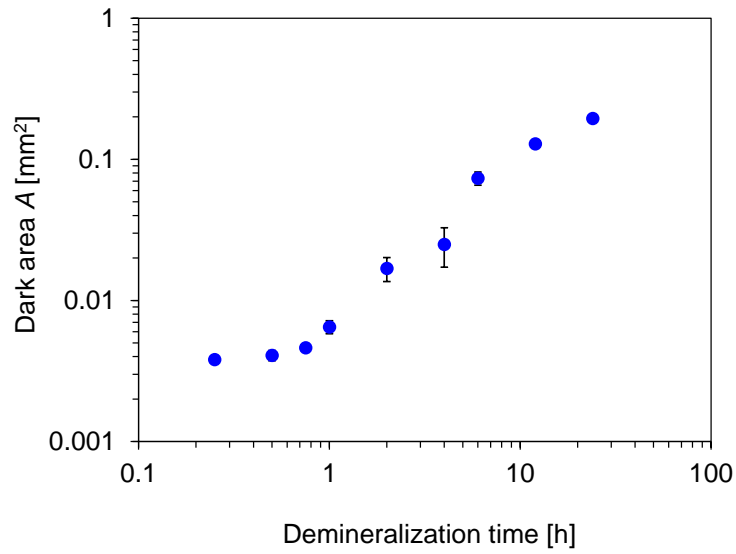
65

Figure 4.6 Changes in the dark area with different demineralization times (0.25, 0.5, 0.75, 1, 2, 4, 6, 12, or 24 h) measured by HAMILTOM. Graph shows the mean and standard deviation of three measurements.

Table 4.1 Dark area and the Vickers hardness of the dentin samples calculated with the calibration curve obtained in group 1.

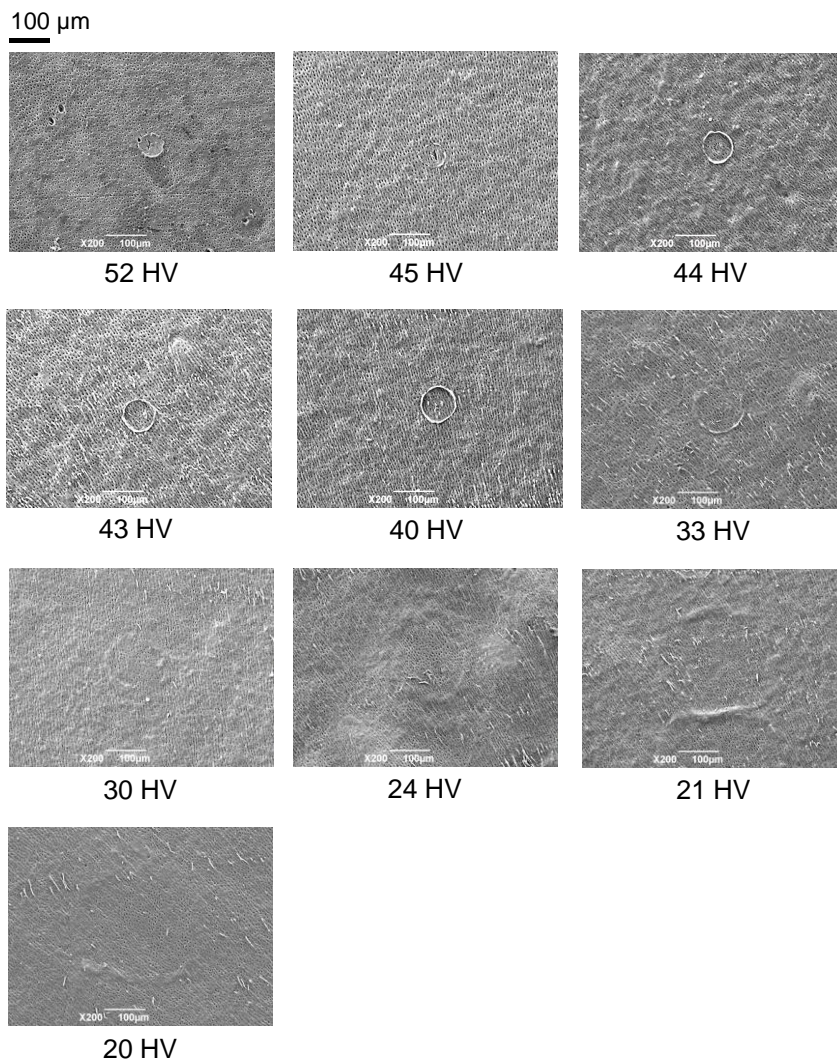|		Demineralization time [h]									
		0	0.25	0.5	0.75	1	2	4	6	12	24
Dark area [mm^2]	Mean	0.0029	0.0038	0.0041	0.0046	0.0065	0.0169	0.0250	0.0736	0.1290	0.1950
	S.D.	0.0024	0.0002	0.0003	0.0003	0.0007	0.0033	0.0078	0.0079	0.0068	0.0080
Vickers hardness [HV]	Mean	52	45	44	43	40	33	30	24	21	20
	S.D.	9	0	1	1	1	1	2	1	0	0

100 µm

Figure 4.7 SEM images of indentations on dentin samples with different Vickers hardness (52, 45, 44, 43, 40, 33, 30, 24, 21, or 20 HV) after hardness measurements with HAMILTOM. The scale bar showed the length of 100 µm.

Figure 4.8 shows the maximum depth of indentations created by the dentin hardness measurement with HAMILTOM at the load of 50 gf for each demineralization time. The average maximum indentation depth ranged from 2.9 to 3.7 µm. The maximum depth of indentation was not changed significantly among the demineralization time from 0 to 24 h, and the demineralization time did not significantly affect the results.
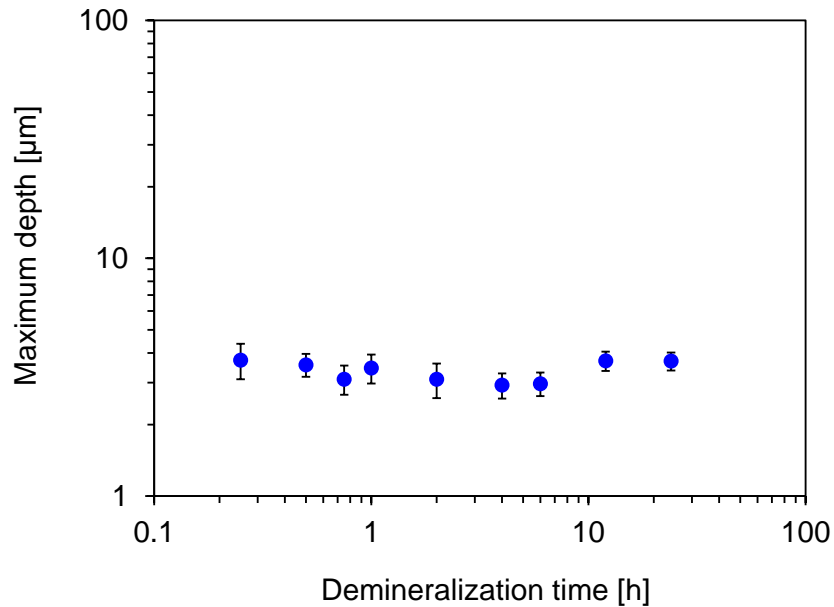
67

Figure 4.8 Changes in the maximum depth of the dentin indentations created by the indenter of HAMILTOM with different demineralization times (0.25, 0.5, 0.75, 1, 2, 4, 6, 12, or 24 h). For the dentin sample with each demineralization time, the maximum depths of three indentations were measured. Graph shows the mean and standard deviation of three measurements.

Figure 4.9 shows the relationship between the dark areas measured by HAMILTOM and the indentation areas measured by the SEM images for each demineralization time. The indentation area of HAMILTOM was calculated as an oval shape by measuring the long and short outer diameters of the indentation from the SEM images. The difference between the dark areas and the indentation areas increased as the demineralization time increased. For demineralization times of 2 hours or less, the dark areas were similar to the indentation areas. On the other hand, the dark areas exceeded the indentation areas significantly for demineralization times more than 2 hours. The difference became more significant with demineralization time.
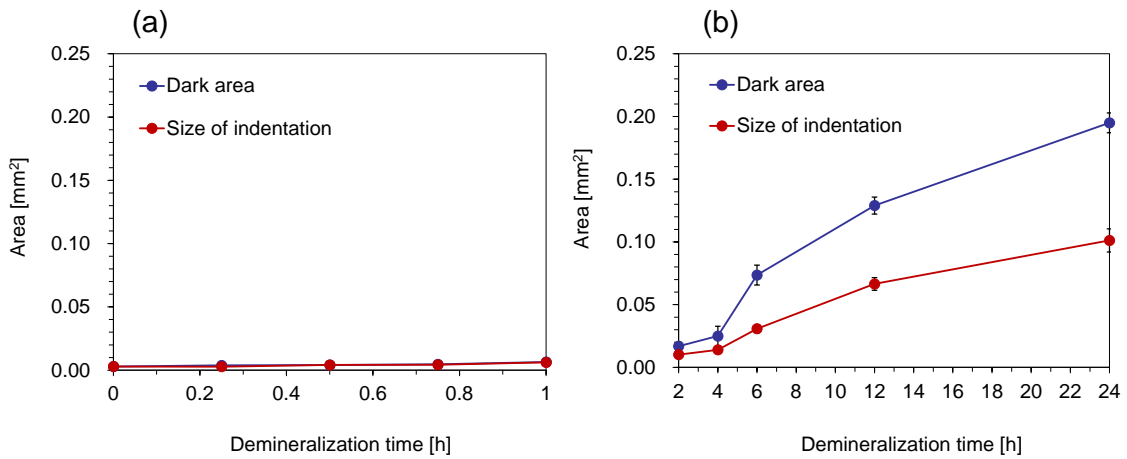
Figure 4.9 Changes in the dark areas measured by HAMILTOM and indentation sizes measured by SEM images with different demineralization times. The indentation sizes were calculated as elliptical shapes by measuring the long and short outer diameters of the indentation from the SEM images (a) Changes as functions of the demineralization time from 0 to 1 h. (b) Changes as functions of the demineralization time from 2 to 24 h. Graphs show the mean and standard deviation of three measurements.

4.4.3 Indentation of HAMILTOM and probe

Figure 4.10 shows SEM images of indentations formed on the sound dentin sample by HAMILTOM with various loads of 100–250 gf and the indentation created by the dental probe based on palpation by the dentist. The indentation areas created by HAMILTOM increased with the increase of the load values. The shapes of indentation created by HAMILTOM was approximately circles. The shape of indentation created by the dental probe because the dentist drew the straight line with the dental, but a scale-like indentation was formed by the operation.

100 µm

10 gf 30 gf 50 gf

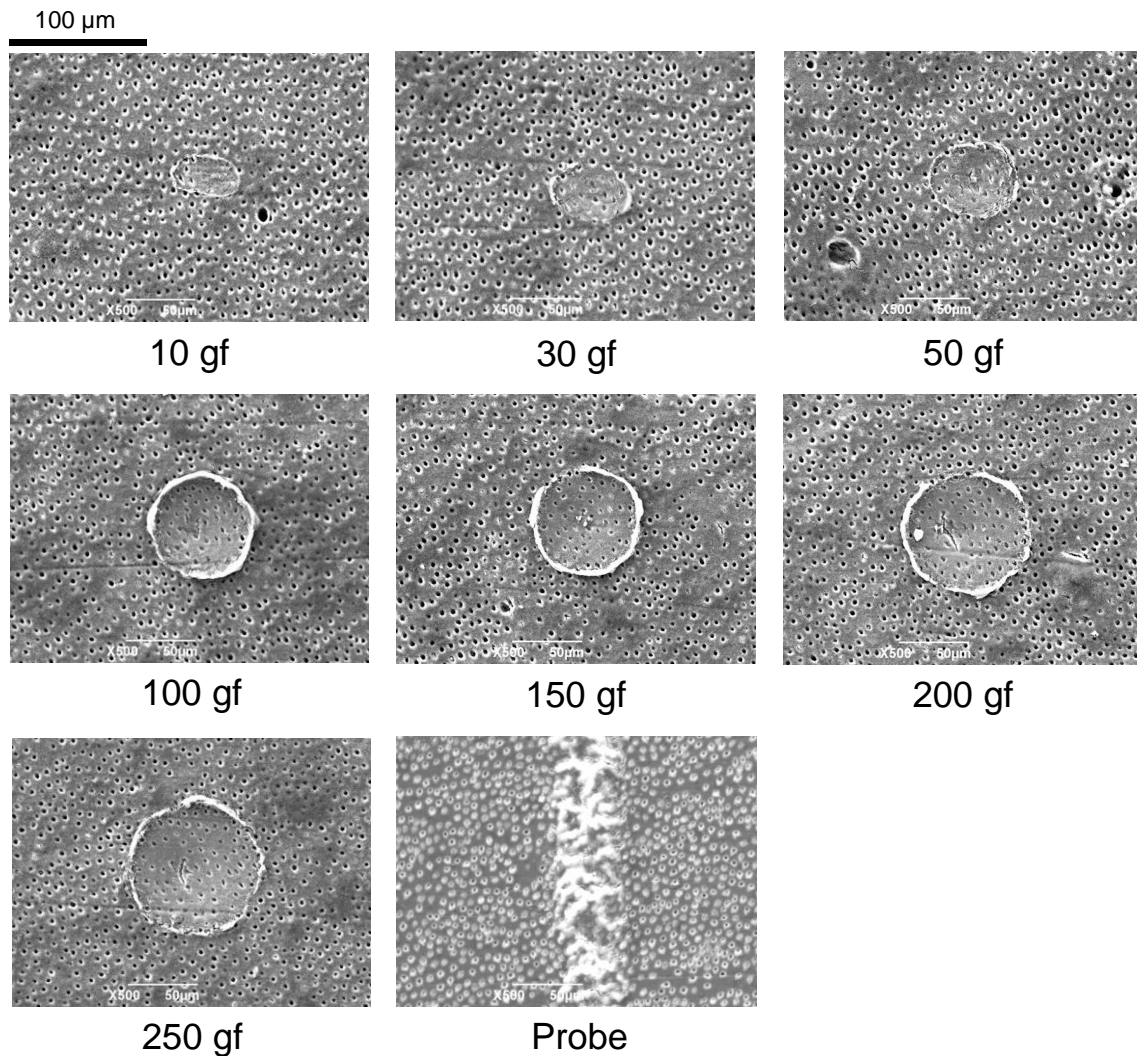100 gf 150 gf 200 gf

250 gf Probe

Figure 4.10 SEM images of indentations on sound dentins with various loads of 10–250 gf using HAMILTOM or the dental probe based on palpation by the dentist belonging to Osaka Dental University. The scale bar showed the length of 100 µm.

Figure 4.11 shows the maximum depths of indentations created by HAMILTOM with various load values from 10 to 250 gf and the dental probe. In Figure 4.11, plots and bars show the mean and standard deviation of three measurements by HAMILTOM, and dotted line and the band show the mean and standard deviation of three measurements by the dental probe. The indentation depths using HAMILTOM increased with load, whereas the indentation depth with the dental probe was 9 µm. The dental probe produced a deeper indentation than that using HAMILTOM for all loads below 250 gf.
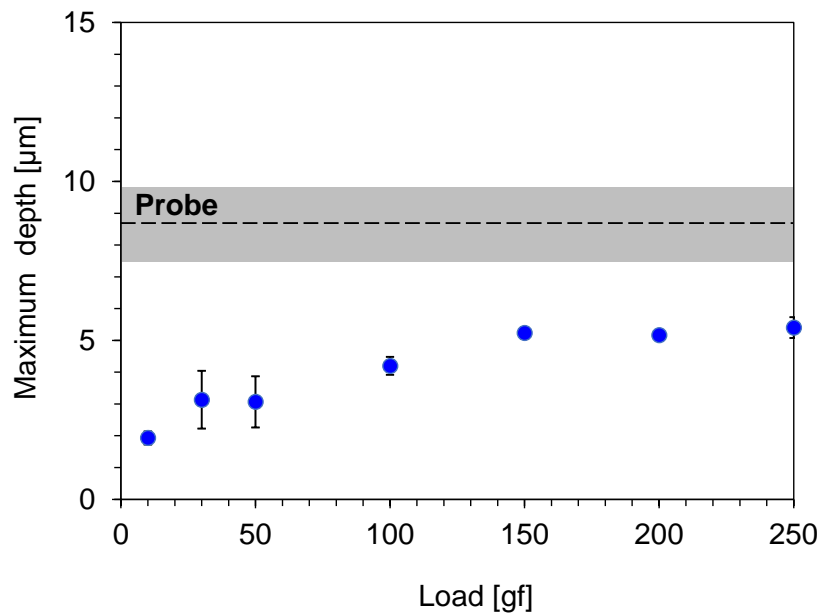

Figure 4.11 Relationship between the maximum depth of indentations on sound dentins created by the hardness measurement by HAMILTOM with the load of 10 to 250 gf and the maximum depth of indentations on sound dentins created by the dental probe. Plots and bars show the mean and standard deviation of three measurements by HAMILTOM. Dotted line and the band show the mean and standard deviation of three measurements by the dental probe.

4.5 Discussion

4.5.1 Mechanism of dentin hardness measurement using HAMILTOM

In this study, the dark areas and the indentation areas measured by the SEM observations for the caries simulated by models with different demineralization times were compared to physically interpret the dentin hardness measured using HAMILTOM. The dark area was almost the same size as the indentation area under the condition of the demineralization time for 2 hours or less. However, the dark area became larger than the indentation area significantly when the demineralization time exceeded 2 hours. This difference between the dark area and indentation area became more pronounced as the demineralization time increased. Thus, it was confirmed the size of the dark area was not the same as the indentation area remained on the dentin sample surface after hardness measurement with HAMILTOM for the caries simulated models.

The significant area difference in the dentin samples with a longer demineralization time is attributed to the water taken into the dentin during the demineralization reaction. Water has a refractive index of 1.34 at a wavelength of 455 nm [96], and the reflectance at the boundary between the indenter and water is much small that the reflected light image at the area where the indenter contacts water is considered to be dark. Caries contains more water than sound dentin [48]. Pushing an indenter into the dentin should exude water from the dentin, increasing the dark area in addition to the deformation of the dentin. Additionally, the dentinal tubules are closed in the indentation of sound dentin formed by HAMILTOM measurements, whereas the tubules are open in the indentation of demineralized dentin samples as shown in Figure 4.7. This provides further evidence that water is more likely to seep from demineralized dentin samples due to the load of the indenter than the sound dentin samples. Elasticity recovery may also contribute to the significant difference between the dark area and indentation area in the caries models for a demineralization time more than 2 hours. No increase in maximum indentation depth with increasing demineralization time was observed in Figure 4.8. It is considered that the dentin sample approached a perfect elastic body and was more likely to recover its elasticity with increasing demineralization time. The deformation gradually rebounds over time. From the SEM image of the indentation by HAMILTOM in Figure 4.7, the indentation is contoured when the demineralization time is 1 hour or less. However, the contour becomes unclear and the contour ridge increases when the demineralization time is two hours or more. The modulus of elasticity of the demineralized dentin is 1.6 GPa, suggesting that it is more easily deformed compared to the sound dentin, which has a modulus of elasticity of 19.5 GPa [97].

4.5.2 Comparison with theoretical formula

The relationship between the theoretical formulas for the projected areas of indenter/material contact by HAMILTOM and Vickers hardness and the actual values measured in the experiments should be discussed for physical interpretation of dark area. Figure 4.12 shows the relationship between the projected areas of indenter/material contact by HAMILTOM and Vickers hardness calculated with the theoretical formulas for the projected areas of indenter/material contact by HAMILTOM shown in Equation (6) and for Vickers hardness shown in Equation (7). 0.49 N was assigned as the load F for the dark areas, and 4.9 N was assigned as the load F for Vickers hardness. The composite elastic modulus E of dentin in the wet condition was assigned to the dark areas, and those of dentin in the dry condition was assigned to the Vickers hardness measured by the previous study [98]. In addition, the elastoplastic parameters P were set to 0.003 for the dark area and 3.2 for the Vickers hardness [98]. The power approximation was fitted for the relationship between HAMILTOM and Vickers hardness from the theoretical formulas.
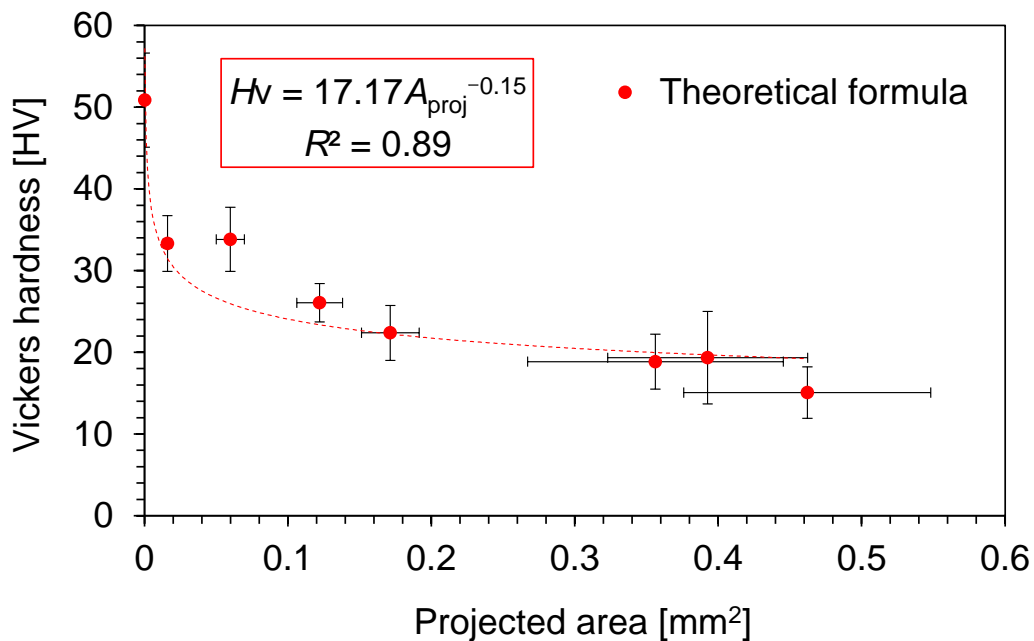

Figure 4.12 The relationship between the projected areas of indenter/material contact by HAMILTOM and Vickers hardness calculated with the theoretical formulas. The projected areas of indenter/material contact by HAMILTOM were calculated from the theoretical formula shown in Equation (6) and the Vickers hardness were calculated from the theoretical formula shown in Equation (7).

Figure 4.13 shows the comparison between the theoretical formulas for the projected areas of indenter/material contact by HAMILTOM and Vickers hardness and the experimental results of HAMILTOM and Vickers hardness. It is important to be noted that the indentation sizes measured by SEM image with different demineralization times shown in Figure 4.9 were used as the dark area since the theoretical formula did not take into account the effect of the exuded water in the dark area. The Vickers hardness was calculated with the calibration curve obtained in group1 in Figure 3.6. It was confirmed that the relationship between the experimental values of the dark area and the Vickers hardness measured in this study showed the same trend of the power approximation as obtained by the theoretical formulas by Figure 4.13. The experimental values of HAMILTOM indentation sizes tended to be smaller than the theoretical values. The experimental values of indentation size might have decreased compared to the dark area measurement due to the elastic recovery of dentin. Therefore, it could be possible to separate the effects of exuded water by the contact of the indenter and the elastic recovery in the difference between the dark area and the indentation area by comparison with the theoretical equation.
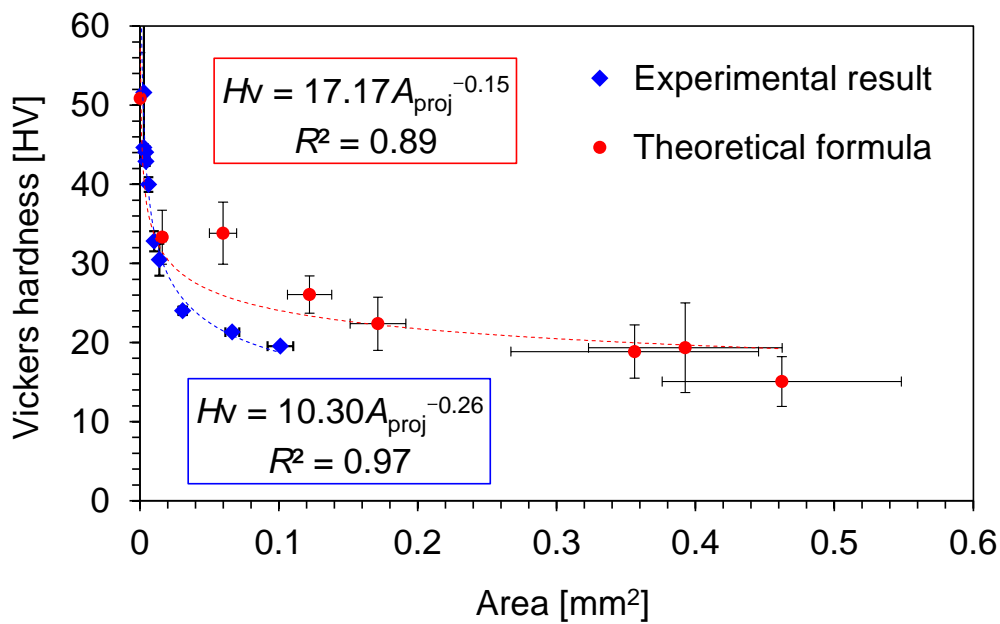

Figure 4.13 The relationship between the indentation area measured by SEM after measurement with HAMILTOM and Vickers hardness and the relationship between the indenter/material projected area and Vickers hardness calculated with the theoretical formulas. Dotted line showed the approximate expression. A determination coefficient was shown.

4.5.3 Invasiveness to dentin of HAMILTOM

The invasiveness of hardness measurement with HAMILTOM needed to be clarified for the clinical use of HAMILTOM, and invasiveness to sound dentin sample of HAMILTOM was evaluated and compared with the conventional dental prove in this study. The indentation depth measured by the confocal laser microscope was very small compared to the depth calculated from the dark area based on the indenter shape used in this study (conical shape with a 90° apex angle) as shown in Figure 4.8, suggesting elastic recovery. Therefore, in samples with a long demineralization time, the elastic recovery of the dentin after the indenter is removed may also contribute to the significant difference between the dark area and the indentation area. Elastic recovery is desirable and may further reduce the indentation size of the demineralized dentin over time. From the perspective of invasiveness, the indentation left after the hardness measurement with HAMILTOM should be small and minimally invasive. Thus, the difference between the dark area measured by HAMILTOM and the actual indentation area may originate from a combination of the water exuded from the dentin due to the insertion of the indenter and elastic recovery of the dentin after removal of the indenter. To accurately interpret the hardness measured using HAMILTOM, each factor should be investigated independently. Dentin emits green fluorescence upon irradiating teeth with excitation light [99]. Consequently, how to isolate each factor using the fluorescence emitted should be investigated as it may be possible to calculate the percentage of dentin deformation in the dark area by fluorescence observations. Additional research should be conducted to discuss the invasiveness of dentin during hardness measurements using HAMILTOM. Comparison of the actual indentation area with the dark area measured by HAMILTOM confirmed that these differ. Since demineralized dentin is often removed after diagnosis, while sound dentin is not, it is critical to consider the invasiveness on sound dentin. The indentation depth by the dental probe with the dentist simulating palpation on sound dentin is more than double that by HAMILTOM with a load of 250 gf in Figure 4.11. Although the probe palpation results in this study are from one dentist and the invasiveness may vary among dentists, the results suggest that HAMILTOM is less invasive than probing during palpation. Here, HAMILTOM defines hardness by measuring the dark area of attenuation at a load of 50 gf, assuming actual clinical use. However, a dentist operating HAMILTOM may apply a load greater than 50 gf. Even at a load of 250 gf, which is significantly higher than the HAMILTOM load of 50 gf, the indentation depth is less than half that of the dental probe, suggesting that HAMILTOM is less invasive than palpation even for practical use in a clinical setting. Hence, HAMILTOM could be minimally invasive.

4.6 Conclusion of this chapter

The study in this chapter physically interpreted the dentin hardness measured using HAMILTOM and considered its measurement mechanism. Additionally, the dentin hardness measurement mechanism and the invasiveness of HAMILTOM measurements on dentin samples were evaluated to clarify the definition of 'Hardness' measured using HAMILTOM and evaluate the safety of HAMILTOM for clinical practical application. The results of the comparison of the dark area measured by HAMILTOM and the size of indentation created on the dentin samples observed by SEM images confirmed that the dark areas were not the size of the indentation suggesting the influence of the water exuded by the contact of the indenter and the elastic recovery of the dentin sample after removal of the indenter were included. A comparison of the indentation depths demonstrated that palpation by a dental probe caused a larger indentation depth than HAMILTOM, suggesting that HAMILTOM was less invasive. Hence, HAMILTOM holds promise as a minimally invasive hardness diagnostic method for root caries.

Chapter 5

Conclusion

Based on the minimal intervention, the new treatment and diagnostic techniques for dental caries using light were developed in this study. This study aimed to develop the treatment with the caries selectivity of removal using the Q-switched Er:YAG laser. Since carious dentin contains more water than sound dentin, caries selective removal could be possible with a laser considered by taking advantage of the difference in absorption spectra due to OH stretching vibrations exhibited by the wavelength of 2.94 µm. The characteristics of laser ablation to dentin slices were examined and compared between the Q-switched Er:YAG laser with a pulse duration of 80–130 ns and the free-running Er:YAG laser with a pulse duration of 200–300 µs without water spray. Furthermore, as the most minimal-intervention approach, the diagnostic method to objectively and quantitatively measure the dentin hardness with a LED light was aimed to prevent unnecessary caries treatment. The demonstration of the basic principle of an optical dentin hardness measurement device using bovine dentin samples with different demineralization times, and the mechanism of dentin hardness measurements using HAMILTOM and the invasiveness to dentin were evaluated.

The study to develop the treatment with the caries selectivity of removal using the Q-switched Er:YAG laser started with the experiments to evaluate the selective removal for caries with the Q-switched Er:YAG laser and compare with the conventional free-running Er:YAG laser. Consequently, the possibility of the selective removal was suggested under certain laser irradiation conditions. However, the condition and progression of caries depends on situations and the dentin hardness needed to be measured essentially to achieve the selective removal for caries because the laser ablation depth and the Vickers hardness was correlated, which suggested the significance of dentin hardness measurement in a clinical setting before caries treatment.

This study developed the dentin hardness measurement method to objectively and quantitatively evaluate the activity and progress of root caries in a clinical setting. With the demonstration of HAMILTOM using bovine dentins with different demineralization times, the correlation between the dentin hardness measured by HAMILTOM and measured by the Vickers hardness tester was confirmed. Moreover, the mechanism of dentin hardness measurements and the invasiveness to dentin were evaluated in this study in order to interpret the dentin hardness measured by

HAMILTOM physically. The results shown in Chapter 3 and 4 suggest that HAMILTOM has the potential of a new diagnostic device for caries and a strong support for the realization of selective removal for caries to measure the dentin hardness in a clinical setting as the most minimal-intervention approach.

References

1.1

[1] World Health Organization (WHO), *Ageing and Health*, https://www.who.int/news-room/fact-sheets/detail/ageing-and-health (2022).

[2] N. J. Kassebaum, E. Bernabé, M. Dahiya, B. Bhandari, C. J. L. Murray, and W. Marcenes, "Global burden of severe tooth loss: a systematic review and meta-analysis," *J. Dent. Res.* **93**(7_suppl), 20S–28S (2014).

[3] 平井義人，寺中敏夫，寺下正道，千田彰. 保存修復学 第5 版. 医歯薬出版 (2012).

[4] Frencken JE, Sharma P, Stenhouse L, Green D, Laverty D, and Dietrich T, "Global epidemiology of dental caries and severe periodontitis – a comprehensive review," *Journal of Clinical Periodontology* **44**.18:S94–S105 (2017).

[5] Marcenes W, Kassebaum NJ, Bernabe E, Flaxman A, Naghavi M, Lopez A, and Murray CJL, "Global burden of oral conditions in 1990–2010," *Journal of Dental Research* **92**:592–597 (2013).

[6] 水谷雄樹. 近年の児童における歯面別う蝕罹患の追跡調査. 口腔衛生会誌 **61**：239–244 (2011).

[7] 平成 28 年度歯科疾患実態調査について，厚生労働省，https://www.mhlw.go.jp/toukei/list/62-28.html (2017).

[8] 安藤雄一，青山旬, 花田信弘. 口腔が健康状態におよぼす影響と歯科保健医療. 保健医療科学 **52**.1:23–33 (2003).

[9] e-ヘルスネット，厚生労働省, https://www.e-healthnet.mhlw.go.jp/information/ (2023)．

1.2

[10] S. O. Griffin, P. M. Griffin, J. L. Swann, and N. Zlobin, "Estimating rates of new rot caries in older adults," *J. Dent. Res.* **83**(8), 634–638 (2004).

[11] D. W. Banting, "The diagnosis of root caries," *J. Dent. Educ.* **65**(10), 991–996 (2001).

[12] D. L. Sumney, H. V. Jordan, and H. R. Englander, "The prevalence of root surface caries in selected populations," *J. Periodontal.* **44**(8), 500–504 (1973).

[13] M. S. Aloranei, A. A. Balhaddad, and M. A. S. Melo, "The burden of root caries: updated perspectives and advances on management strategies," *Gerodontology* **38**(2), 136–153 (2021).

[14] E. A. A. Neel, A. Aljabo, A. Strange, S. Ibrahim, M. Coathup, A. M. Young, L. Bozec, and V. Mudera, "Demineralization remineralization dynamic in teeth and bone," *Int. J. Nanomed.* **11**, 4743–4763 (2016).

[15] M. Goldberg, A. B. Kulkarni, M. Young, and A. Boskey, "Dentin: structure, composition and

mineralization: the role of dentin ECM in dentin formation and mineralization." *Front. Biosci. Elite Ed.* E3(2), 711–735 (2011).

[16] F. Driessens, "Mineral aspects of dentistry," *Monogr. Oral Sci.* **10**, 1–215 (1982).

1.3

[17] 日本歯科保存学会. う蝕治療ガイドライン 第1 版. 永末書店 (2009).

[18] Tyas MJ, Anusavice KJ, Frencken JE, and Mount GJ, "Minimal intervention dentistry – a review," *Int. Dent. J.* **50**：1–12 (2000).

[19] 総山孝雄，田上順次. 保存修復学総論. 永末書店：21–53 (1996).

[20] 吉山昌宏，桃井保子. う蝕治療のミニマルインターベンションクインテッセンス出版 44–53 (2004).

[21] 岩見行晃，清水亜矢子，山本洋子，川上克子，伊藤祥作，高橋雄介，藪根敏晃，金子智之，恵比須繁之. 齲蝕検知液を用いた齲蝕除去法の客観性についての臨床的評価，日歯保存誌 **47**：716–722 (2004).

1.4

[22] T. Kita, K. Ishii, K. Yoshikawa, K. Yasuo, K. Yamamoto, and K. Awazu, "Selective removal of carious dentin using nanosecond pulsed laser at a wavelength of 5.85 μm; relationship between hardness and ablation property," *Jpn. Soc. Laser Dent.* **25**(1) 2–7 (2014).

1.5

[23] Y. Momoi, S. Kubo, and M. Fukushima, "Clinical Strategies of Root Caries," pp. 66–77, Quintessence Publishing, Japan (2018).

[24] The Japanese Society of Conservative Dentistry, "Caries Treatment Guideline 3rd edition; Root Caries Treatment Guideline," pp. 44–46, Nagasue syoten (2020).

[25] M. Fukushima, "Perspective of root surface caries treatment in operative dentistry," *Jpn. J. Conserv. Dent.* **62**(2) 92–98 (2019).

[26] B. Rosén, D. Birkhed, K. Nilsson, G. Olavi, and J. Egelberg, "Reproducibility of clinical caries diagnoses on coronal and root surfaces," *Caries Res.* **30**(1), 1–7 (1996).

2.1.1

[27] 松本光吉. 歯科用Er:YAGレーザーの基礎と臨床. 口腔保健協会 3 (2008).

[28] Goldman L, Hornby P, Meyer R, and Goldman B. *Nature* **203**：417 (1964).

[29] Stern RH, Sognnaes RF. *J. Dent. Res.* **43**：873 (1964).

[30] Stern RH, Vahl J, and Sognnaes RF, "Laser enamel: ultrastructural observations of pulsed carbon dioxide laser effects," *J. Dent. Res.* **51**：455–460 (1972).

[31] Hall RR, "The healing of tissues excised by a carbon-dioxide laser," *Br. J. Surg.* **58**：222– 225 (1971).

[32] Pecaro BC, Garehime WJ, "The CO_2 laser in oral and maxillofacial surgery," *J. Oral Maxillofac. Surg.* **41**：725–728 (1983).

[33] Frame JW, Das Gupta A, Dalton G, and Rhys Evans P, "Use of the carbon dioxide laser in the management of premalignant lesions of the oral mucosa," *J. Laryngol. Otol.* **98.**12：1251–1260 (1984).

[34] Leo J Miserendino, Rovert M Pick, Tuda Tadamasa. Laser in Dentistry，第1版，クインテッセンス出版 (2004).

[35] Pick RM, Colvard MD, "Current status of lasers in soft tissue dental surgery," *J. Periodontol* **64.7**：589–602 (1993).

[36] Hibst R, Keller U. "Experimental studies of the application of the Er:YAG laser on dental hard substances: I. Measurement of the ablation rate," *Lasers Surg. Med.* **9.4**：338–344 (1989).

[37] 茅野照雄, 落合聡, 清野和夫, 山本肇, 中島貞洋, 望月孝晏. Erbium:YAG レーザー照射ヒト抜去歯の病理組織学的変化について. 口病誌 **56**：381–392 (1989).

[38] Takamori K, Furukawa H, Katayama T, and Watanabe S, "Basic Study on Vibrations of Tooth Preparations Caused by Air Turbin, Quintuple Speed Handpiece, and Er:YAG laser," *Laser in Dentistry, International Congress Series* **1248**:227–230 (2003).

[39] 瀧澤雅一, 青木聡, 高瀬保晶, 石川達也, 熊崎護, 井上昌孝, 善入邦男, 藤井弁次, 長谷川紘司, 石川烈. Er:YAG Laserの窩洞形成への応用と臨床評価. 日歯保存誌 **38**:1035–1047 (1995).

[40] Kato J, Moriya K, Jayawardena JA, and Wijeyeweera RL, "A clinical application of Er:YAG laser for cavity preparation in children," *J Clin Laser Med Surg*, **21**:151–156 (2003).

[41] Keller U, Hibst R, Geurtsen W, Schilke R, Heidemann D, Klaiber B, and Raab WHM, "Erbium:YAG laser application in caries therapy. Evaluation of patient perception and acceptance," *J. Dent.* **26**.8：649–656 (1998).

[42] Taniguchi Y, Aoki A, Mizutani K, Takeuchi Y, Ichinose S, Takasaki AA, Schwarz F, and Izumi Y, "Optimal Er:YAG laser irradiation parameters for debridement of microstructured fixture surfaces of titanium dental implants," *Lasers Med Sci* **29**:1057–1068 (2013).

[43] Aoki A, Sasaki K, Watanabe H, and Ishikawa I, "Lasers in nonsurgical periodontal therapy," *Periodontology 2000.* **36**:59–97 (2004).

[44] Ishikawa I, Aoki A, and Takasaki A, "Potential applications of erbium:YAG laser in periodontics," *J. Periodont. Res.* **39**:275–285 (2004).

[45] Ishikawa I, Aoki A, Takasaki K, Mizutani K, Sakaki KM, and Izumi Y, "Application of lasers in periodontics: true innovation or myth?," *Periodontol 2000.* **50**:90–126 (2009).

[46] Aoki A, Mizutani K, Schwarz F, Sculean A, Yukna RA, Takasaki AA, Romanos GE,

Taniguchi Y, Sasaki KM, Zeredo JL, Koshy G, Coluzzi DJ, White JM, Abiko Y, Ishikawa I, and Izumi Y, "Periodontal and peri-implant wound healing following laser therapy," *Periodontol 2000.* **68**:217–269 (2015).

[47] Mizutani K, Aoki A, Coluzzi D, Yukna RA, Wang CY, Pavlic V, and Izumi Y, "Lasers in minimally invasive periodontal and peri-implant therapy," *Periodontol 2000*. **71**:185–212 (2016).

2.1.2

[48] Wigdor HA, Walsh JT Jr, Featherstone JDB, Visuri SR, Fried D, and Waldvogel JL. *Lasers* Surg. Med. **16**：103–133 (1995).

[49] 瀧澤雅一，天谷哲也，高橋賢，清野栄治，高瀬保晶，平井義人，石川達也. Er:YAGレーザーの窩洞形成への応用コンポジットレジンとの適合性について. 接着歯学**16**:24–33 (1998).

[50] Visuri SR, Gilbert JT, Wright DD, Wigdor HA, and Walsh JT Jr, "Shear strength of composite bonded to Er:YAG laser-prepared dentin," *J. Dent. Res*. **75**:599–605 (1996).

[51] Armengol V, Jean A, Rohanizadeh R, and Hamel H, "Scanning electron microscopic analysis of diseased and healthy dental hard tissues after Er:YAG laser irradiation: *in vitro* study," *J. Endod*. **25**:543–546 (1999).

[52] Neves AA, Coutinho E, De Munck J, and Van Meerbeek B. *J. Dent*. **39**:154–162 (2011).

[53] Celiberti P, Francescut P, and Lussi A, "Performance of four dentine excavation methods in deciduous teeth," *Caries Res* **40**:117–123 (2006).

[54] 天谷哲也，平井義人. Er:YAGレーザー照射後における修復処置. 日レ歯誌 **16**:105–110 (2005).

[55] Erhardt MCG, Toledano M, Osorio R, and Pimenta LA. *Dent. Mater.* **24**:786–798 (2008).

[56] 横田啓太，岩田有弘，保也謙三，吉川一志，山本一世. Er:YAGレーザーによる歯質切削に関する研究. 日本歯科保存学雑誌. **57**.1：9–18 (2014).

2.1.3

[57] De Moor RJ, Meire M, Goharkhay K, Moritz A, and Vanobbergen J, "Efficacy of ultrasonic versus laser-activated irrigation to remove artificially placed dentin debris plugs," *J Endod* **36**(9): 1580–1583 (2010).

[58] Takizawa M, Amagai T, Haruyama C, Kameyama A, Takase Y, Hirai Y, and Kumazaki M, "Effects of water spray amounts on dentin cutting with Er:YAG laser irradiation," *J Dent* **12**(2):84–91 (2001).

[59] Celiberti P, Francescut P, and Lussi A, "Performance of four dentine excavation methods in deciduous teeth," *Caries Res* **40**:117–123 (2006).

[60] Yan R, Chan KH, Tom H, Simon J, Darling CL, and Fried D, "Selective removal of dental

caries with a diode-pumped Er: YAG laser," In: *Lasers in Dentistry* XXI, vol 9306. International Society for Optics and Photonics, p 93060O (2015).

[61] Shimizu K, Ishii K, Hashimura K, Yoshikawa K, Yasuo K, Yamamoto K, and Awazu K, "Selective removal of demineralized dentin by nanosecond-pulsed laser at wavelength of 2.94 μm," *Rev Laser Eng* **44**:182–186 (2016).

[62] Buyukhatipoglu I, Ozsevik AS, Secilmis A, and Usumez A, "Effect of dentin laser irradiation at different pulse settings on microtensile bond strength of flowable resin," *Dent Mater J* **35**(1): 82–88 (2016).

[63] Delmé KIM, De Moor RJG, "Scanning electron microscopic Evaluation of enamel and dentin surfaces after Er: YAG laser preparation and laser conditioning," *Photomed Laser Surg* **25**(5):393–401 (2007).

[64] Trevelin LT, Marques MM, Aranha ACC, Arana-Chavez VE, and Matos AB, "Effect of super short pulse E r: YAG laser on human dentin - scanning electron microscopy analysis," *Microsc Res Tech* **78**(6):472–478 (2015).

[65] Jelinkova H, Dostalova T, Němec M, Koranda P, Miyagi M, Iwai K, Shi Y-W, and Matsuura Y, "Free-running and Q-switched Er:YAG laser dental cavity and composite resin restoration," *Laser Phys Lett* 4(11):835–839 (2007).

2.2.1

[66] Kita T, Ishii K, Yoshikawa K, Yasuo K, Yamamoto K, and Awazu K, "*In vitro* study on selective removal of bovine demineralized dentin using nanosecond pulsed laser at wavelengths around 5.8 μm for realizing less invasive treatment of dental caries," *Lasers Med Sci.* **30**:961–967 (2015).

[67] Henschel CJ, "Heat impact of revolving instruments on vital dentin tubules," *J Dent Res* **22**(4):323–333 (1943).

2.3.3

[68] De Cruz A, Andreotti A, Ceccarini A, and Colombini MP, "Laser cleaning of works of art: evaluation of the thermal stress induced by Er:YAG laser," *Appl Phys B Lasers Opt* **117**:533–541 (2014).

[69] Pohto M, Scheinin A, "Microscopic observations on living dental pulp II. The effect of thermal irritants on the circulation of the pulp in the lower rat incisor," *Acta Odontol Scand* **16**(3):315–327 (1958).

[70] Zach L, Cohen G, "Pulp response to externally applied heat. Oral Surgery," *OralMed Oral Pathol* **19**(4):515–530 (1965).

2.5.1

[71] Guillot-Noel O, Roman RGS, and Perriere J, "Growth of apatite films by laser ablation: reduction of the droplet areal density," *Appl Phys* **80**:1803–1808 (1996).

[72] Kato J, Shinoki T, Awazu K, and Moriya K, "A to Z guide to dental laser treatment," Ishiyaku Publishers, Tokyo (2003).

[73] Yasuda G, Inage H, Takamizawa T, Kurokawa H, Rikuta A, and Miyazaki M, "Determination of elastic modulus of deminer alized resin-infiltrated dentin byself-etch adhesives," *Eur J Oral Sci* **115**(1):87–91 (2007).

[74] Ogawa K, Yamashita Y, Ichijo Y, and Fusayama T, "The ultrastructure and hardness of the transparent of human carious dentin," *J Dent Res* **62**(1) (1993).

2.5.4

[75] K. Ishii, T. Kita, K. Yoshikawa, K. Yasuo, K. Yamamoto, and K. Awazu, "Selective removal of carious human dentin using a nanosecond pulsed laser operating at a wavelength of 5.85 μ m." *J. Biomed. Opt.* **20**(5), 051023-051023(2015).

3.1.1

[76] J. Arends and J. J. T. Bosch, "Demineralization and remineralization evaluation techniques," *J. Dent. Res.* **71**(3_sppl), 924–928 (1992).

[77] J. J. T. Bosch and B. Angmar-Mansson, "A review of quantitative methods for studies of mineral content of intra oral incipient caries lesions," *J. Dent. Res.* **70**(1), 2–14 (1991).

3.1.2

[78] RH. Selwitz, AI. Ismail, and NB Pitts, "Dental caries", *Lancet* **369** (9555) 51–59 (2007).

[79] "Caries Risk Assessment and Management," American Dental Association. 9 June 2021.

[80] World Health Organization (WHO), Oral Health Surveys, Basic Methods, 5th Edition, ISBN 978 92 4 154864 9, 1–137 (2013).

[81] NB. Pitts, R. Kim, Ekstrand, and ICDAS Foundation, "International Caries Detection and Assessment System (ICDAS) and its International Caries Classification and Management System (ICCMS)–methods for staging of the caries process and enabling dentists to manage caries," *Community Dent. Oral Epidemiol.* **41**(1) 41–52 (2013).

[82] M. Fukushima, "Perspective of root surface caries treatment in operative dentistry," *Jpn. J. Conserv. Dent.* **62**(2) 92–98 (2019).

[83] A. Shimizu, and Y. Torii, "Research on spoon excavator 2nd report; Relationship between sharpness and sharpening ability of spoon excavator cutting edge," *Jpn. J. Conserv. Dent.* **28**(2), 690-694 (1985).

[84] A. Shimizu, S. Nakashima, T. Nikaido, T. Sugarawa, T. Yamamoto, and Y. Momoi, "Newly developed hardness testing system, "Cariotester": Measurement principles and development of a program for measuring Knoop hardness of carious dentin," *Dent. Mater. J.* **32**(4), 643–647 (2013).

3.2.1

[85] R. A. Harper, R. M. Shelton, J. D. James, E. Salvati, C. Besnard, A. M. Korsunsky, and G. Landini, "Acid-induced demineralisation of human enamel as a function of time and pH observed using X-ray and polarised light imaging," *Acta Biomater.* **120**, 240–248 (2021).

[86] H. C. Margolis and E. C. Moreno, "Composition and cariogenic potential of dental plaque fluid," *Crit. Rev. Oral biol. Med.* **5**(1), 1–25 (1994).

3.2.3

[87] "SCHOTT Optical glass datasheet 517642.251," https://www.schott.com/en-us/products/optical-glass-p1000267/downloads

[88] Z. Meng, X. S. Yao, H. Yao, Y. Liang, T. Liu, Y. Li, G. Wang, and S. Lan, "Measurement of the refractive index of human teeth by optical coherence tomography," *J. Biomed. Opt.* **14**(3), 034010 (2009).

3.5.1

[89] J. D. B. Featherstone, "Dental caries: a dynamic disease process," *Aust. Dent. J.* **53**(3), 286–291 (2008).

[90] S. Sánchez-García, H. Reyes-Morales, T. Juárez-Cedillo, C. Espinel-Bermúdez, F. Solórzano-Santos, and C. García-Peña, "A prediction model for root caries in an elderly population," *Community Dent. Oral Epidemiol.* **39**(1), 44–52 (2011).

3.5.2

[91] L. Angker, C. Nockolds, M. V. Swain, and N. Kilpatrick, "Correlating the mechanical properties to the mineral content of carious dentine—a comparative study using an ultra-micro indentation system (UMIS) and SEMBSE signals," *Arch. Oral Biol.* **49**(5) 369–378 (2004).

[92] V. Fuentes, M. Toledano, R. Osorio, and R. M. Carvalho, "Microhardness of superficial and deep sound human dentin," *J. Biomed. Mater. Res. A.* **66**(4), 850–853 (2003).

4.1.2

[93] NB Pitts, "Diagnostic tools and measurements--impact on appropriate care," *Community Dent. Oral Epidemiol.* **25**(1) 24–35 (1997).

4.2.4

[94] 逆井基次: "圧子力学," (2017).

[95] Li Xingguo, An Bingbing, and Zhang Dongsheng: "Determination of elastic and plastic mechanical properties of dentin based on experimental and numerical studies," *Appl. Math. Mech.* (English Ed.) **36**(10), 1347–1358(2015).

4.5.1

[96] G. M. Hale and M. R. Querry, "Optical constants of water in the 200-nm to 200-μm wavelength region," *Appl. Opt.* **12**(3), 555–563 (1973).

[97] MK. Pugach, J. Strother, CL. Darling, D. Fried, SA. Gansky, SJ. Marshall, and GW. Marshall, "Dentin caries zones: mineral, structure, and properties," *J. Den. Res*. **88**(1), 71–76 (2009).

4.5.2

[98] 三好悠斗：卒論 (2021).

4.5.3

[99] T. Hasegawa, "Possibility of Light-induced Fluorescence Application for the Clinical Diagnosis and Treatment of Dentin Caries," *Dental Med Res*. **33**(3), 259–264 (2013).

Acknowledgements

Accomplishment Report

Peer-Reviewed Papers

1. **S. Kondo**, H. Hazama, K. Tanaka, A. Kasakawa, S. Sekine, S. Akiyama, K. Awazu: "*In vitro* study on nanosecond-pulsed *Q*-switched Er:YAG laser-induced selective removal for caries dentin," Lasers in Dental Science **4**, 195–202 (2020).

2. A. Kasakawa, S. Sekine, K. Tanaka, J. Murakami, **S. Kondo**, H. Hazama, K. Awazu, S. Akiyama: "Effect of *Q*-switched Er:YAG laser irradiation on bonding performance to dentin surface," Dental Materials Journal **41**(4), 616–623 (2022).

3. **S. Kondo**, H. Hazama, Y. Tomioka, A. Mine, S. Yamaguchi, S. Okumura, H. Tanimoto, K. Yasuo, K. Yoshikawa, K. Yamamoto, K. Awazu: "Demonstration of an optical dentin hardness measuring device using bovine dentin with different demineralization times," Journal of Biomedical Optics **27**(10), 105004-1–105004-13 (2022).

4. **S. Kondo**, Y. Tomioka, N. Fujimoto, A. Mine, S. Yamaguchi, S. Okumura, H. Tanimoto, K. Yasuo, K. Yoshikawa, K. Yamamoto, H. Hazama: "Mechanism of dentin hardness measurements using an optical dentin hardness measuring device," Journal of Biomedical Optics, under review.

Non Peer-Reviewed paper

1. <u>近藤 聡太</u>, 間 久直, 冨岡 穣, 峯 篤史, 山口 哲, 奥村 瑳恵子, 谷本 啓彰, 保尾 謙三, 吉川 一志, 山本 一世, 粟津 邦男: "脱灰時間を変化させたウシ象牙質による光学式歯質硬さ測定装置の基本原理実証," 電気学会光・量子デバイス研究会資料, OQD-23-005, pp. 23–28, 2023.

Domestic Conferences

[Oral presentations (Non peer-reviewed)]

1. <u>近藤 聡太</u>, 間 久直, 清水 公太, 田中 健司, 谷口 あや, 関根 伸一, 秋山 茂久, 粟津 邦男: "齲蝕の選択的治療に向けた*Q*スイッチEr:YAGレーザーによる象牙質切削特性の評価," レーザー学会学術講演会第37回年次大会 (徳島, 2017年1月9日).

2. 笠川 [谷口] あや, 関根 伸一, 田中 健司, <u>近藤 聡太</u>, 吉田 輝稔, 間 久直, 粟津 邦男, 秋山 茂久: "*Q*スイッチEr:YAGレーザー照射が象牙質表面へもたらす影響," 第31回日本レーザー歯学会総会・学術大会 (大阪, 2019年10月5日).

3. <u>近藤 聡太</u>, 間 久直, 冨岡 穣, 峯 篤史, 山口 哲, 奥村 瑳恵子, 谷本 啓彰, 保尾 謙三, 吉川 一志, 山本 一世, 粟津 邦男: "脱灰時間を変化させたウシ象牙質による光学式歯質

硬さ測定装置の基本原理実証,” 電気学会 光・量子デバイス研究会 ～バイオメディカルフォトニクス応用～ (東京, 2023年3月27日).

[Poster presentations (Non peer-reviewed)]

1. 谷口 あや, 関根 伸一, 田中 健司, <u>近藤 聡太</u>, 間久直, 粟津 邦男, 秋山 茂久: “象牙質に対するQ スイッチEr:YAG レーザーの照射がレジン接着システムに及ぼす影響,” 第29 回日本レーザー歯学会総会・学術大会 (新潟, 2017年9月23日).

2. 谷口 あや, 関根 伸一, 田中 健司, <u>近藤 聡太</u>, 間 久直, 粟津 邦男, 秋山 茂久: “平均パワー密度60W/cm2 の Q スイッチEr:YAG レーザー照射が象牙質およびレジン接着に及ぼす影響,” 第30 回記念日本レーザー歯学会総会・学術大会 (東京, 2019年10月21日).

3. <u>近藤 聡太</u>, 間 久直, 谷口 あや, 関根 伸一, 田中 健司, 秋山 茂久, 粟津 邦男: “Q スイッチEr:YAG レーザー照射象牙質に対するレジン接着のメカニズムに関する研究,” 第30 回記念日本レーザー歯学会総会・学術大会 (東京, 2019年10月21日).

4. 田中 健司, 関根 伸一, 笠川 [谷口] あや, 吉田 輝稔, <u>近藤 聡太</u>, 間久直, 粟津邦男, 秋山 茂久: “ヒト口腔扁平上皮癌由来細胞に対する5-アミノレブリン酸を用いたPDD の検討,” 第 31 回日本レーザー歯学会総会・学術大会 (大阪, 2019年10月6日).

5. <u>近藤 聡太</u>, 冨岡 穰, 峯 篤史, 山口 哲, 奥村 瑳恵子, 谷本 啓彰, 保尾 謙三, 吉川 一志, 山本 一世, 間 久直: “光学式歯質硬さ測定装置による象牙質硬さ測定のメカニズム,” 第 35 回日本レーザー歯学会総会・学術大会 (東京, 2023年11月26日).